AIAA JOURNAL
Vol. 45, No. 12, December 2007

Jet-into-Crossflow Boundary-Layer Control: Innovation in Gas Turbine Blade Cooling

Kh. Javadi,* M. Taeibi-Rahni,† and M. Darbandi‡
Sharif University of Technology, 11365 Tehran, Iran

DOI: 10.2514/1.28770

Jet into crossflow has numerous technological applications, such as in film cooling of gas turbine blades. It has been more than half a century that people have been studying this problem and research is still underway due to its importance and its complexities. This paper is a computational study concerned with film cooling of gas turbine blades. A novel near-wall flow control technique of using staggered arrangement of small injection ports near a film-cooling hole (combined triple jet) is introduced. The fluid injected from the small ports changes the flow pattern downstream, resulting in a considerable enhancement of cooling efficiency. The flowfield computations, governed by the Reynolds-averaged Navier–Stokes equations (incorporating the Reynolds stress turbulence model), were performed using the SIMPLE algorithm on a nonuniform staggered grid. The results show that, due to the introduction of new counter-rotating vortex pairs, this approach provides considerable improvement in 1) film-cooling efficiency, 2) uniform distribution of the coolant film, 3) reduction of the mixing strength between the freestream and the coolant jets, and 4) reduction of skin friction drag. In addition, qualitative comparison of our results with those of regular staggered holes arrangement indicated that this new technique has a considerably higher film-cooling performance.

Nomenclature

a_1	=	constant in shear stress transport turbulence model
C_2, C_1, & C_s	=	empirical constants in Reynolds stress transport model
$\overline{C_f}$	=	spanwise-averaged skin friction drag coefficient
C_{ij}	=	convection terms in Reynolds stress transport model
c_1', c_2', & c_μ	=	empirical constants in Reynolds stress transport model
D	=	jet hydraulic diameter, 12.7 mm
D_{ij}^L	=	molecular diffusion tensor in Reynolds stress transport model
D_{ij}^T	=	turbulent diffusion tensor in Reynolds stress transport model
F_1, F_2	=	switching functions in κ-ω model
F_{ij}	=	production tensor by system rotation
G_{ij}	=	buoyancy tensor
J	=	momentum ratio, $(\rho_{\text{jet}} V_{\text{jet}}^2)/(\rho_{\text{cf}} V_{\text{cf}}^2)$
k	=	turbulence kinetic energy
P_{ij}	=	production tensor in Reynolds stress transport model
Pr_l	=	laminar Prandtl number
Pr_t	=	turbulent Prandtl number
p/D	=	spanwise jets spacing
$R = V_{\text{jet}}/V_{\text{cf}}$	=	jet-to-crossflow velocity ratio, 0.5
Re	=	Reynolds number, 4700
s/D	=	streamwise jets spacing
T	=	temperature
$\overline{U_i}$	=	mean velocity components
U_i	=	instantaneous velocity components
u_i	=	fluctuative velocity components
V_{cf}	=	crossflow velocity, 11 m/s
V_j	=	jet velocity, 5.5 m/s
β, β^*, γ	=	empirical constants in shear stress transport turbulence model
ε	=	turbulence energy dissipation rate
ε_{ij}	=	energy dissipation rate tensor
$\eta = (T_{\text{aw}} - T_{\text{cf}})/(T_{\text{jet}} - T_{\text{cf}})$	=	film-cooling effectiveness
$\bar{\eta}$	=	spanwise-averaged film-cooling effectiveness
μ	=	viscosity coefficient
μ_t	=	eddy-viscosity coefficient
ρ	=	density
σ_k, σ_ω, $\sigma_{\omega 2}$	=	empirical constants in shear stress transport turbulence model
σ_k	=	Prandtl number
$\tau_{ij} = -\rho\overline{u_i u_j}$	=	Reynolds stress tensor
ω	=	specific dissipation rate, $\varepsilon/\beta^* k$

Subscripts

cf	=	designates crossflow
jet	=	designates jet
aw	=	adiabatic wall

Presented as Paper 5272 at the 35th AIAA Fluid Dynamics Conference and Exhibit, Toronto, Ontario, June 6-9, 2005, 6 June–6 September 2005; received 12 November 2006; revision received 25 February 2007; accepted for publication 29 March 2007.

*Ph.D. Student, Aerospace Engineering Department, Post Office Box 11365-8639; also Aerospace Research Institute (Ministry of Science, Research, and Technology), Post Office Box 15875-3885, 15875 Tehran, Iran; khjavadi@mehr.sharif.edu.

†Associate Professor, Aerospace Engineering Department, Post Office Box 11365-8639; also Aerospace Research Institute (Ministry of Science, Research, and Technology), Post Office Box 15875-3885, 15875 Tehran, Iran; Taeibi@sharif.edu.

‡Associate Professor, Aerospace Engineering Department, Post Office Box 11365-8639; Darbandi@sharif.edu.

I. Introduction

THE jet-into-crossflow problem has been under investigation for more than six decades [1]. This problem appears in many applications, such as boundary-layer control (using suction/blowing), film cooling of gas turbine blades, gas discharge from VSTOL aircraft, rockets into the atmosphere, etc. Because of the interaction of the jet with the crossflow, a highly complex and three-dimensional flowfield is produced in the jet near field. Such vortical flow is characterized by both large-scale coherent structures and small-scale

turbulence, and the mixing process is controlled by the dynamics of these structures. Some of the large-scale coherent structures can be identified as counter-rotating vortex pairs (CRVP), horseshoe vortices, wake flow, weak boundary-layer vortices, secondary vortices beneath the CRVP, multilayer shear flow, wall-jet flow, and other vortices downstream of the injected jet [2–7]. Also, this problem is a highly complicated and nonhomogenous flow with multiple length, velocity, and time scales [8]. Accurate prediction of the jet penetration and the separation zone are strongly dependent on correct simulation of such structures, which are crucial from heat transfer and film-cooling effectiveness points of view. Many people have attempted to predict the physics of this problem, using different approaches, such as eddy-viscosity models, Reynolds stress transport models (RSM), large-eddy simulation (LES), etc. The abilities of different turbulence models for the problem considered here depend on the jet-into-crossflow characteristics, the sensitivity of the flow quantities, and the flow locations [9–16]. Various researchers have tried to improve the use of these models [13–15]. It seems that the RSM has many more capabilities and seems to be less sensitive to the flow locations (also to the jet-into-crossflow characteristics; however, they are computationally much more expensive) [17–19]. On the other hand, some people have used the LES approach to simulate this problem and their results seem to be optimistic [20–22].

As far as the application of jet-into-crossflow in cooling of the gas turbine blades is concerned, note that a considerable increase in the thrust and in the cycle efficiency of gas turbines can be achieved through higher turbine entrance temperatures. However, the increased inlet temperature can result in material failure of the turbine blades due to higher heat loads and thermal stresses. On the other hand, the life span of gas turbine blades can be increased drastically through their proper cooling. In high-performance gas turbine engines, film cooling is extensively used to cool the turbine components' surfaces exposed to hot gases coming from the combustion chamber.

Since 1950, when Eckert and Livingood [23] first introduced the film-cooling technique, many people have studied this problem and observed many physical and geometrical quantities affecting film-cooling efficiency. Some of the most important ones are discussed here:

1) Mass flux ratio quantities (blowing ratio) [5,9,24–26]: Relatively low values of blowing ratio R are beneficial for a suitable film-cooling effectiveness. A common range of R for industrial applications is $R = 0.5$–1. Lower values are not safe to protect the surfaces and higher values cause too much flow penetration into the crossflow boundary layer, resulting in too much interaction and mixing, which are not suitable from a film-cooling standpoint.

2) Injection angle [24–38]: The injection angle plays a crucial role in film-cooling effectiveness. The penetration of coolant jets into a hot crossflow boundary layer, the mixing process, the flow separation, and wake formation after the coolant jet are highly dependent on the jet injection angle. It is preferred to use compound-oriented jets compared to those with streamwise injection ($\beta = 0$ deg) or normal injection ($\alpha = 90$ deg). Note that the common values of compound-oriented angle are $\beta \equiv 30$–60 deg, whereas relatively lower values of α (20–45 deg) are suitable in practical situations.

3) Hole shape [4,26,38–46]: The vortical flow generated downstream of the jet and the interactions between the coolant jet and the hot crossflow are severely affected by the jet hole shapes. For instance, slowly curved outward holes have higher film-cooling effectiveness (this is more obvious in higher blowing ratios).

4) Length to diameter of the jet channel [47–51]: The jet entrance flow characteristics not only have significant effects on film-cooling effectiveness, but also the quality of the flowfield at the jet exit which depends strongly on the jet channel length. The separation of the flow near the entrance due to the sharp corner of the holes or due to the effects of the crossflow can considerably affect the jet exit profile and thus the cooling effectiveness. Note that this effect is higher for shorter lengths of the jet channel.

5) Jet array arrangements (single or double rows) [28,33,34,52–72]: Two of the most important keys in protecting the surfaces from high-temperature hot gases are the suitable coolant jet's locations and their arrangements over the surfaces. For the same geometry and for the same flow characteristics, a staggered arrangement of jet arrays has higher overall film-cooling effectiveness compared with the regular (in-line) arrangement. The staggered arrangement helps the jets to recover for each other, leading to a more uniform coolant film distribution.

6) Jet holes streamwise or spanwise spacing [41,63,72]: Spanwise and streamwise jet spacing are also important parameters in film cooling. Common values of p/D and s/D are between three and six. It should be pointed out that their larger values cannot fully protect the surface, whereas their smaller values can cause structural difficulties.

7) Jet and crossflow Reynolds numbers [31,40]: Both the jet and the crossflow Reynolds numbers can strongly affect the characteristic length, velocity, and time scales of such flow and thus affect flow separation, size of different eddies, film-cooling effectiveness, etc.

8) Density ratio [24–27,31,44,73,74]: Depending on the momentum flux ratio, there exists three different situations: the jet remains attached to the surface, it detaches and then reattaches, or it fully detaches. Spanwise-averaged film-cooling effectiveness depends on density and momentum ratios. Decreases in density ratio and increases in momentum ratio both significantly reduce the spreading of the film-cooling jet and thereby reduce the spanwise-averaged effectiveness. However, for the same blowing ratio, increasing the density ratio improves the cooling effectiveness.

9) Jet and crossflow turbulence intensity [40,47,75–79]: The turbulence intensity considerably enhances the mixing of the coolant jet with the main hot crossflow, which is not suitable from a film-cooling point of view. High mainstream turbulence level has little effect at low-blowing ratios. Increasing the mainstream turbulence level to about 20% has no effect at low-blowing ratios, for which the coolant jets remain attached to the surface. At high-blowing ratios, however, for which the coolant jets are somewhat detached, high mainstream turbulence level causes a decrease in film-cooling effectiveness. This decrease is consistent with an increase in the dispersion of the coolant jet by the mainstream.

10) Compressibility effects and shock/boundary layer/jet interactions [80–85]: The interactions between shock waves and film cooling affect the magnitudes of local and spanwise-averaged film-cooling effectiveness distribution. Local and spanwise-averaged effectiveness are generally higher when shock waves are present if a film plenum condition (with zero crossflow Mach number) is used. The effectiveness values measured in a supersonic approaching freestream with shock waves decrease, as the injection crossflow Mach number increases. Such changes are due to the altered flow separation regions, different injection velocity distributions, and alterations of static pressure at the jet exits (produced by different types of shock wave events). Generally speaking, weak shock waves do not reduce film-cooling effectiveness, whereas stronger ones do.

Careful review of related literature indicates that many studies have been conducted to understand the physical phenomena regarding the film-cooling problem. Particularly, they have tried to achieve more suitable jet exit configurations for providing more surface protection with minimal amount of coolant fluid. In this work, we introduce a completely new approach for controlling the interactions between the jets and the crossflow and thus to improve the amount of film-cooling effectiveness and its uniform distribution. The basis of this idea goes back to our previous studies [86–90], wherein the significant role of mixing zone in such flow was noted. In our new approach, a novel near-wall flow control technique of using a staggered arrangement of small injection ports near a film-cooling hole is proposed. The fluid injected from these small jets changes the flow pattern downstream, resulting in considerable enhancement of cooling efficiency. Using this new approach has shown to have many advantages, including 1) improvement of the film-cooling effectiveness, 2) achievement of a much more uniform film-cooling distribution, 3) reduction of the mixing strength between the hot crossflow and the coolant jets, and 4) reduction of the skin friction drag. Note, contrary to previous works, whose intentions had been improving film-cooling efficiency through complex geometrical

means (complex injection angle, complex hole shapes, etc.), in this work we achieve considerably higher cooling efficiency using a relatively simple hole geometry (squared) and injection angle (90 deg).

II. Governing Equations

The governing equations are the Reynolds-averaged conservation of mass, momentum, and energy for a stationary incompressible flow, as

$$\frac{\partial \overline{U_i}}{\partial x_i} = 0 \tag{1}$$

$$\rho \frac{\partial \overline{U_j U_i}}{\partial x_j} = -\frac{\partial p}{\partial x_i} + \frac{\partial}{\partial x_j}\left[\mu\left(\frac{\partial \overline{U_i}}{\partial x_j} + \frac{\partial \overline{U_j}}{\partial x_i}\right)\right] + \frac{\partial}{\partial x_j}(-\rho \overline{u_i u_j}) \tag{2}$$

$$\rho \frac{\partial}{\partial x_j}(\overline{U_j T}) = \frac{\partial}{\partial x_j}\left\{\left(\frac{\mu_l}{\mathrm{Pr}_l} + \frac{\mu_t}{\mathrm{Pr}_t}\right)\frac{\partial \bar{T}}{\partial x_j}\right\} \tag{3}$$

where, $\rho \overline{u_i u_j}$ are the Reynolds stresses which need to be modeled. As mentioned earlier, because this problem has multiple characteristic scales, the eddy-viscosity models are not suitable enough to fully predict the physics of such flows. Hence, the RSM, which has a higher potential to simulate such complex flows, was used here as

$$\underbrace{\frac{\partial}{\partial x_k}(\rho \overline{U_k}\,\overline{u_i u_j})}_{C_{ij}=\text{convection}} = \underbrace{-\frac{\partial}{\partial x_k}[\rho \overline{u_i u_j u_k} + \overline{p(\delta_{kj}u_i + \delta_{ik}u_j)}]}_{D_{ij}^T=\text{turbulent diffusion}}$$
$$+ \underbrace{\frac{\partial}{\partial x_k}\left[\mu \frac{\partial}{\partial x_k}(\overline{u_i u_j})\right]}_{D_{ij}^L=\text{molecular diffusion}} + \underbrace{p\left(\overline{\frac{\partial u_i}{\partial x_j}} + \overline{\frac{\partial u_j}{\partial x_i}}\right)}_{\phi_{ij}=\text{pressure strain}} \underbrace{-\rho\left(\overline{u_i u_k}\frac{\partial \overline{U_j}}{\partial x_k} + \overline{u_j u_k}\frac{\partial \overline{U_i}}{\partial x_k}\right)}_{P_{ij}=\text{stress production}}$$
$$\underbrace{-\rho\beta(g_i\overline{u_j\theta} + g_j\overline{u_i\theta})}_{G_{ij}=\text{buoyancy production}} \underbrace{-2\mu\left(\overline{\frac{\partial u_i}{\partial x_k}} + \overline{\frac{\partial u_j}{\partial x_k}}\right)}_{\varepsilon_{ij}=\text{dissipation}} \underbrace{-2\rho\Omega_k(\overline{u_j u_m}\varepsilon_{ikm} + \overline{u_i u_m}\varepsilon_{jkm})}_{F_{ij}=\text{production by system rotation}} \tag{4}$$

Note, C_{ij}, D_{ij}^L, P_{ij}, and F_{ij} do not require any modeling, whereas D_{ij}^T, G_{ij}, ϕ_{ij}, and ε_{ij} do. Many people, such as Pope [8], Launder and Shima [91], Daly and Harlow [92], Hanjalic and Launder [93], Launder et al. [94], Gibson and Launder [95], Lumley and Khajeh-Nouri [96], Fu et al. [97], etc., have made many attempts to model these terms. Also, Hwang and Jaw [98] have reviewed some variations of the second-moment closure models to show their capabilities and limitations.

In this work, the shear stress transport turbulence model (SST), which is a combination of the k-ω and the k-ε models, was used to close the RSM equations. The equations used in the SST model are as follows:

$$\frac{\partial(u_j k)}{\partial x_j} = \tau_{ij}\frac{\partial \overline{U_i}}{\partial x_j} - \beta^* \rho\omega k + \frac{\partial}{\partial x_j}\left[(\mu + \sigma_k \mu_t)\frac{\partial k}{\partial x_j}\right] + 2\rho(1 - F1)\sigma_{\omega 2}\frac{1}{\omega}\frac{\partial k}{\partial x_j}\frac{\partial \omega}{\partial x_j} \tag{5}$$

$$\frac{\partial(u_j \omega)}{\partial x_j} = \frac{\gamma}{\nu_t}\tau_{ij}\frac{\partial \overline{U_i}}{\partial x_j} - \beta\rho\omega^2 + \frac{\partial}{\partial x_j}\left[(\mu + \sigma_\omega \mu_t)\frac{\partial \omega}{\partial x_j}\right] \tag{6}$$

where ω is the specific dissipation rate and τ_{ij} is the Reynolds stress tensor. The turbulent kinematics viscosity ν_t is

$$\nu_t = \frac{a_1 k}{\max(a_1\omega, SF_2)} \tag{7}$$

where,

$$S = \left[\left(\frac{\partial \overline{U_i}}{\partial x_j} + \frac{\partial \overline{U_j}}{\partial x_i}\right)\frac{\partial \overline{U_i}}{\partial x_j}\right]^{1/2} \tag{8}$$

The switching function F_1 is such that it is unity near the surface and zero away from it, resulting in use of the κ-ω model near the wall and the κ-ε model in the remainder of the flowfield. The values of the constants $\sigma_k, \sigma_\omega, \sigma_{\omega 2}, \beta, \beta', \gamma$, and the relations defining the switching functions, F_1, F_2, and a_1 are given by Menter [99].

III. Physical Domain and Boundary Conditions

We have used different domains based on the ordinary or the new film-cooling approaches. The boundary conditions used are inlet, outlet, no flux, periodic (or symmetric), and solid wall.

A. Ordinary Film-Cooling Physical Domain

For code validation purpose, our single jet results are compared with those of a squared jet normally injected into a crossflow (Fig. 1), which is the experimental (LDV) and numerical (standard k-ε) works of Ajersch et al. [9]. Their jet hydraulic diameter (jet width D) was 12.7 mm and their jet Reynolds number (based on D) was 4700 with a uniform speed of 5.5 m/s at the entrance of the jet channel. Note, they used three blowing ratios of 0.5, 1.0, and 1.5, whereas we only used $R = 0.5$ (a more common value in film-cooling applications). Here, the dimensionless jet channel's length was $5D$ and the crossflow region was extended from $5D$ upstream to $40D$ downstream (from the center of the jet). Also, in the lateral direction, the domain extends to $20D$ above the wall.

B. Physical Domain of the New Film-Cooling Approach

In this work, a novel near-wall flow control technique of using a staggered arrangement of small injection ports near a film-cooling hole have been considered. To be able to compare the results of this work with the ordinary film-cooling approach, the same amount of total coolant air and the same cross-sectional area were used (Fig. 1). Note that other parameters, such as the size of the physical domain and the inlet jet and the crossflow velocities (blowing ratio), were taken to be the same as the ordinary film-cooling case. However, the jet Reynolds number was different (e.g., Re is 4030 for the main coolant jet).

C. Boundary Conditions

In this work, five different types of boundary conditions, namely inflow, outflow, no flux, solid wall, and periodic (or symmetric) were used as follows:

1) *Inflow boundary condition:* At the inlet, the boundary layer thickness was set to $2D$ to match the benchmark data [9]. For the boundary layer at the inlet plane of the main flow, the one-seventh power-law profile was used for the x-velocity component, whereas a uniform streamwise velocity was implemented above $y = 2D$ and other velocity components were set to zero. The value of turbulent kinetic energy was taken from the experimental data of Ajersch et al. [9]. Note, $\sqrt{k}$ was about 1.2% of V_{cf} and the maximum turbulent kinetic energy in the boundary layer was on the order of 10% of V_{cf}. The values of Reynolds stress terms are calculated from $\overline{u_i' u_j'} = a\kappa$. Because turbulence is nonisotropic here, the values of $a = 1$ for $i = j = 1$, $a = 1/2$ for $i = j = 2, 3$, and $a = 0$ for $i \neq j$ were used [100].

The inlet turbulence energy dissipation rate can be obtained from the following relation [15,99]:

$$\omega_{\mathrm{in}} = \frac{(1 \to 10)V_{\mathrm{cf}}}{L} \tag{9}$$

where L is the approximate length of the physical domain. At the channels inlet, uniform velocity and turbulent kinetic energy distributions were assumed.

2) *Outflow boundary condition:* Zero gradients of the flow quantities were used at the outflow boundary. Also, to ensure mass conservation during SIMPLE iterations, we used the following relation for the streamwise velocity component:

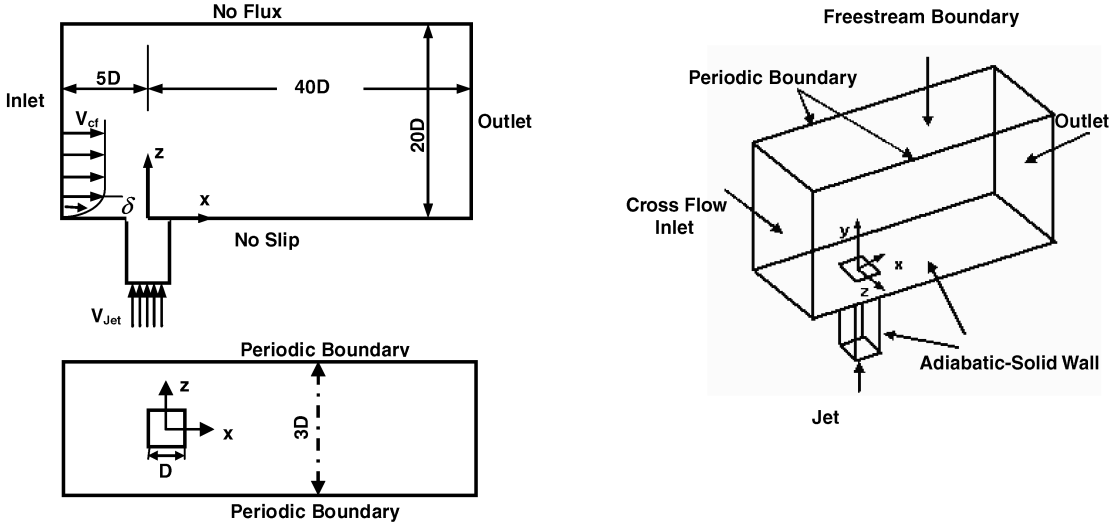

a)

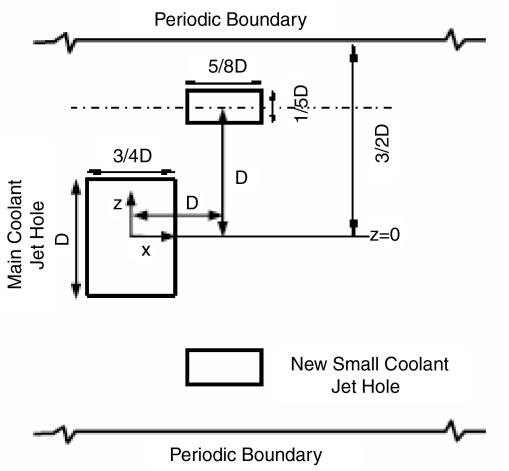

b)

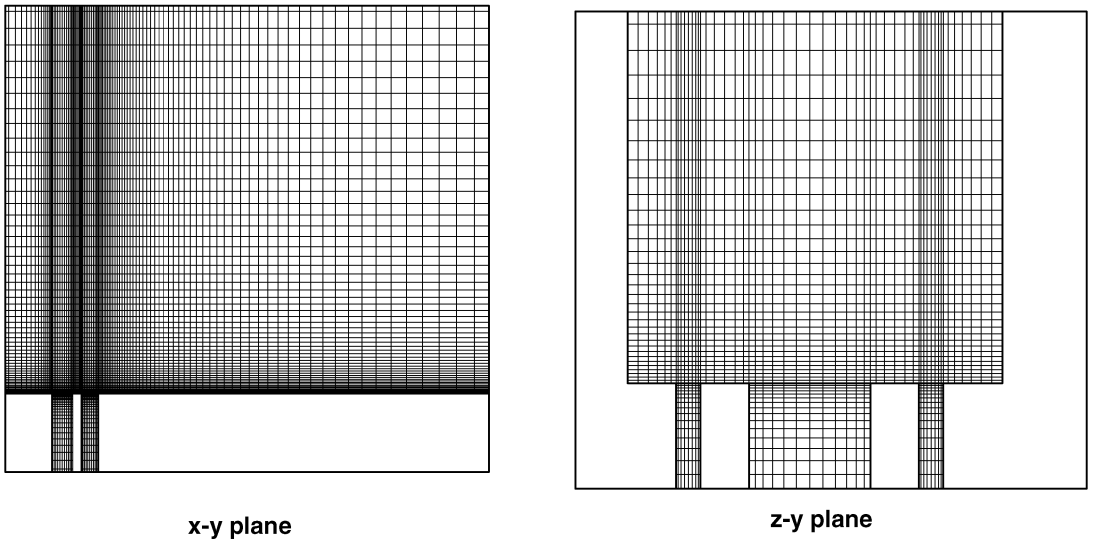

c)

Fig. 1 Physical domain and boundary conditions used a) ordinary film cooling, b) CTJ, and c) grid used.

$$\bar{u}_{NI,J,K} = \bar{u}_{NI-1,J,K}(\dot{M}_{\text{in}}/\dot{M}_{\text{out}}) \tag{10}$$

where, $\dot{M}_{\text{in}}$ and $\dot{M}_{\text{out}}$ are the inlet and outlet mass flow rates, respectively.

3) *No-flux boundary condition:* At infinitely far from the wall, no-flux boundary conditions were used as

$$\frac{\partial \phi}{\partial n} = 0 \tag{11}$$

where n is the direction normal to the face.

4) *Periodic boundary condition:* In this work, it was assumed that there are infinite numbers of coolant jets in the spanwise direction. To

consider the effects of the neighboring jets, the periodic boundary condition was used as

$$\phi_{i,j,1} = \phi_{i,j,NK-1}; \qquad \phi_{i,j,NK} = \phi_{i,j,2} \tag{12}$$

However, because we used a staggered grid, the periodic boundary condition for the z-velocity component was

$$w_{i,j,2} = w_{i,j,NK-1}, \qquad w_{i,j,NK} = w_{i,j,3} \tag{13}$$

5) *Solid wall boundary condition:* No-slip and adiabatic-wall boundary conditions were used at the solid walls. Also, for the SST model, turbulence kinetic energy was set to zero at the wall and ω was obtained from the following relation, suggested by Menter [99]:

$$\omega = 60\upsilon/\beta_1(\Delta y_1)^2 \tag{14}$$

where Δy_1 is the distance to the next point away from the wall, υ is the molecular kinematics viscosity, and β_1 is a constant.

To calculate the Reynolds stress terms near the wall, an explicit wall boundary condition was used. Using the equilibrium assumption and neglecting the convection and diffusion terms in Eq. (4), the Reynolds stresses at the cells adjacent to the wall were found to be

$$\frac{\overline{uu}_\varsigma}{k} = 1.1, \qquad \frac{\overline{uu}_\xi}{k} = 0.25, \qquad \frac{\overline{uu}_\lambda}{k} = 0.65, \qquad \frac{\overline{u_\varsigma u_\xi}}{k} = -0.26 \tag{15}$$

where ς, ξ, and λ are tangential, normal, and binormal axes in local coordinate system used, respectively [95].

IV. Computational Methodology

Here, the three-dimensional, incompressible, and stationary flowfield computations, governed by the Reynolds-averaged Navier–Stokes (RANS) equations (incorporating the RSM with the SST model for its closure), were performed using the SIMPLE algorithm on a nonuniform staggered grid. The numerical method used was finite volume, employing a hybrid scheme. The size of the grid used was $140 \times 72 \times 56$ for the main flow, $12 \times 32 \times 12$ for the main jet, and $12 \times 32 \times 8$ for the small jets in x, y, and z directions, respectively (see Fig. 1c for details of grid spacing). Also, other equations, such as the Reynolds stress transport and the turbulent kinetic energy (and the energy dissipation rate) were solved segregately. Finally, a line-by-line three-diagonal matrix algorithm (TDMA) was used to solve the discretized algebraic equations with appropriate underrelaxation factor.

V. Code Validation and Verification

Because of the lack of experimental data for the combined-triple-jet (CTJ) problem, we validated our computer code with the ordinary film-cooling system (one jet only). The hydrodynamic results were compared with those (numerical and experimental) of Ajesch et al. [9], whereas the temperature field was compared with those of Mahjoob and Taeibi-Rahni [39]. In this section, there is a brief discussion on code validation and then the results of the CTJ problem are verified by grid refinement study and by convergence and outlet mass flow rate histories.

As shown in Figs. 2 and 3, there are many complex three-dimensional vortical structures in jet-into-crossflows, such as wake flow, separation, horseshoe vortices, etc. As Fig. 2b demonstrates, the flow begins to accelerate and a multilayer shear flow and a wall jet begin to form approximately at $x/D = 1$ near the surface. However, slightly above the wall jet, we observe a deceleration region, leading to a wake flow. At locations $x/D = 3$ and $x/D = 5$, Fig. 3 shows the

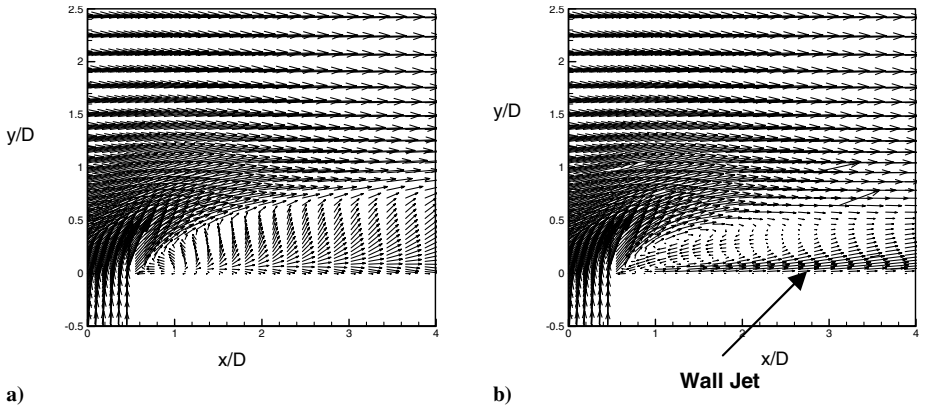

Fig. 2 Velocity vectors downstream of the jet hole at a) $z/D = 0$ and b) $z/D = -0.25$.

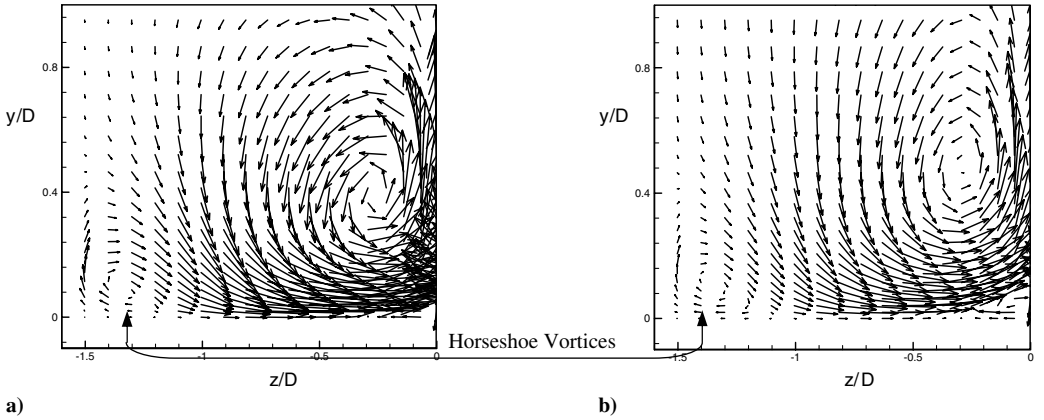

Fig. 3 CRVPs and horseshoe vortices at: a) $x/D = 3$ and b) $x/D = 5$.

horseshoe vortices generated downstream of the jet which disappear further downstream.

The mean streamwise velocity profiles at locations $x/D = 0$ and 3 are shown in Fig. 4. As shown in this figure, the mean streamwise velocity predicted by all turbulence models at $x/D = 0$ are very close and have good agreements with the experimental results of [9]. However, as shown in Fig. 4b, further downstream of the jet, i.e., $x/D = 3$, various turbulence models give considerably different results (with superiority of the RSM model).

Figure 5 illustrates the transverse component of the mean velocity for $z/D = -0.5$ at two different locations: $x/D = 0$ and $x/D = 3$ ($x/D = 0$ and $z/D = -0.5$ is just the edge of the jet hole). The crossflow over the jet acts like a ceiling and does not permit the jet to penetrate into the crossflow boundary layer. This causes the jet flow to spread in transverse direction. As shown in Fig. 5b, the transverse velocity profile in this region is positive near the wall and negative away from it. This demonstrates the formation of a wake region and a spiral flow at this location. Also, it can be seen from this figure that, in the wake region, the flow near the wall moves faster. All turbulence models used here have almost the same ability for predicting this phenomenon.

Figure 6 demonstrates the shear Reynolds stress profile of $-\overline{uv}$ at the jet center plane for two different locations $x/D = 1$ and $x/D = 3$. As shown in this figure, the maximum value is at the wall-jet region (Fig. 2) which is the consequence of a high-velocity gradient there. It is clear from this figure that the standard k-ε model is the weakest model in predicting the turbulence stresses there. This may be due to the use of the wall function in this model, whereas the k-ω and the SST models use an explicit boundary condition at the wall. On the other hand, the RSM model has excellent capability to predict

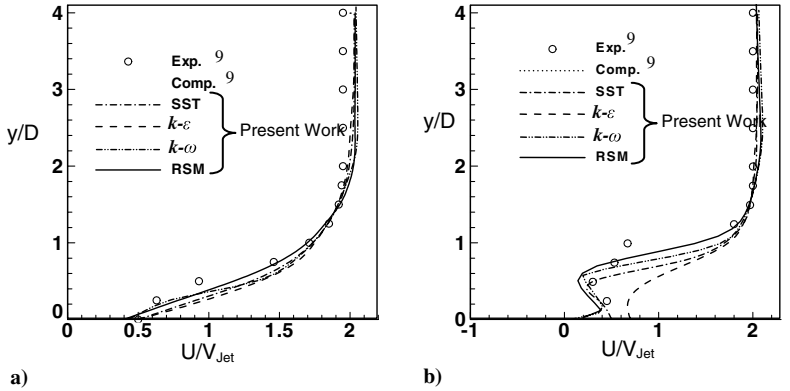

Fig. 4 Comparison of the mean streamwise velocity at jet center plane a) $x/D = 0$ and b) $x/D = 3$.

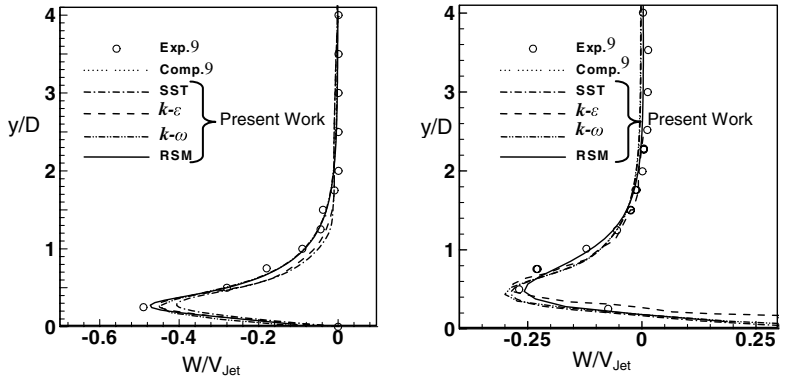

Fig. 5 Comparison of the transverse velocity component at $z/D = -0.5$ and a) $x/D = 0$, b) $x/D = 3$.

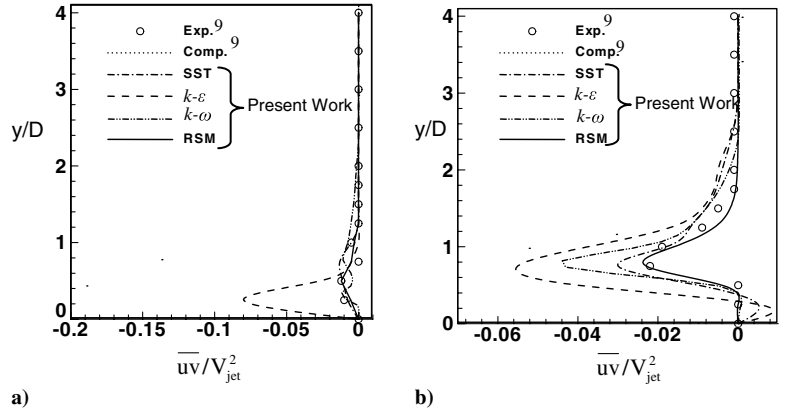

Fig. 6 Comparison of the shear stress profiles at the jet center plane for a) $x/D = 1$ and b) $x/D = 3$.

turbulent shear stresses at different flow locations. The following discussions explain why the RSM model has a higher capability in predicting such flows.

From the transport equation for $-\overline{uv}$, one notes that one of the main production terms for generation of $-\overline{uv}$ is $-\overline{v^2}\partial U/\partial y$, which is the result of the interactions between the mean velocity gradient and the turbulent shear Reynolds stresses. According to Anderpolus and Rodi [3], eddy-viscosity models should, in principle, be able to represent the shear stress distribution in the flow regimes where $-\overline{uv}$ and $\partial U/\partial y$ are generally of opposite signs. However, one example when such models fail is when streamline curvatures and the influence of $\partial V/\partial x$ become significant. This certainly occurs in the jet near field, where the freestream flow accelerates around the jet. In direct turbulence models (RSM), there are certain terms which inherently take care of certain flow physics. For instance, in boundary-layer flows, the only term which contributes to the production term in k and ε equations is $-\rho uv\partial U/\partial y$, whereas in conditions where the flow accelerates and/or decelerates, the irrotational strains ($\partial U/\partial x$, $\partial V/\partial y$, $\partial W/\partial z$) become important [101]. Also, Thompson and Whitelaw [102] found that near separation points (as well as in the separation zones), the production term $-\rho(\overline{u^2}-\overline{v^2})\partial U/\partial x$ is of equal importance compared with the aforementioned terms. Curvature (wall or streamline) is known to have significant effects on turbulence. Also, the entire Reynolds stress tensor is active in the interaction process between shear stresses, normal stresses, and mean velocity gradients. Thus, when predicting the flow, where curvature effects are important, it is necessary to use turbulence models which accurately predict all Reynolds stresses (not only the shear stresses) [101].

As is shown in Figs. 2–5, jet-into-crossflow problems include acceleration/deceleration, wakes, highly swirling/rotating with strong streamline curvature and backflow regions. Most two-equation turbulence models fail to simulate most of these phenomena accurately. However, as the exact form of the production terms are used in the second-moment closure models (such as RSM), the production due to the irrotational strains is correctly accounted for and thus, these models are able to respond to curvature effects and acceleration/deceleration regions more properly [103,104].

In summary, whenever nonisotropic effects are present, one should consider using the RSM, because the exact forms of the production terms are used which can respond to these nonisotropic effects properly. Some examples in which nonisotropic effects are often important are flows with strong curvature, swirling flows, flows with strong acceleration/deceleration, etc. Most of these phenomena appear in jet-into-crossflow problems. Because of these important considerations, we used the RSM in our simulations.

In addition to the preceding validation, we also compared our results with the numerical results of Mahjoob and Taeibi-Rahni [39], in which they used the STAR-CD commercial software. Figure 7a compares the film-cooling effectiveness in the centerline plane with those of Mahjoob and Taeibi-Rahni [39]. This figure shows close agreements between the two results. Also, as a rough comparison, the spanwise-averaged film-cooling effectiveness is compared with some previous experimental works [35–37,54]. As shown in Fig. 7b, there are close agreements between these results as well.

Table 1 Number of grid points used in the main flow for five different cases

Case	NI	NJ	NK	Total
1	70	36	28	70,560
2	140	36	28	141,120
3	140	72	28	282,240
4	140	72	56	564,480
5	210	72	66	997,920

Table 2 Number of grid points used in the main jet channel for five different cases

Case	NI	NJ	NK	Total
1	6	16	6	576
2	6	32	6	1152
3	12	32	6	2304
4	12	32	12	4608
5	16	32	16	8192

Table 3 Number of grid points used in small jet channels for five different cases

Case	NI	NJ	NK	Total
1	6	16	4	384
2	6	32	4	768
3	12	32	4	1536
4	12	32	8	3072
5	16	32	12	6144

Besides the preceding code validation, in this section we make further evaluation of the code by studying grid refinement and inlet/outlet mass flow rate and convergence histories for the CTJ problem.

To investigate the effects of grid refinement in our CTJ solutions, we have used five different nonuniform grids, which were clustered near the walls (as well as near the jet holes). To satisfy the wall boundary condition assumed here [Eq. (14)], the grid spacing at the first cell above the wall was taken to be such that its y^+ was less than three [99]. Tables 1–3 show the total grid points used in each direction for the main flow, for the main jet exit, and for the small jet exits, respectively. Grid independency was achieved when the maximum deviations in the U-velocity component (at $x/D = 5$, $z/D = 0$) and the spanwise-averaged film-cooling effectiveness downstream of the jets were less than 2 and 0.5%, respectively. Moreover, the results of a sensitive flow variable (turbulent kinetic energy) were used to compare the five different grids examined. Figure 8a shows the turbulent kinetic energy profile at the jet center plane and $x/D = 5$. As shown in this figure, all cases show the same trend. However, the results of the fourth and the fifth cases are considerably closer. Therefore, the fourth case was considered in our simulation. Figure 8b illustrates the mass flow rate history at the inlet

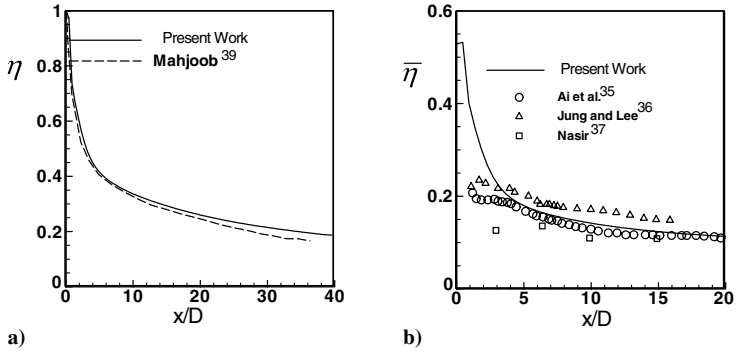

Fig. 7 Comparison of the film-cooling effectiveness with a) Mahjoob and Taeibi-Rahni [39] and b) [35–37].

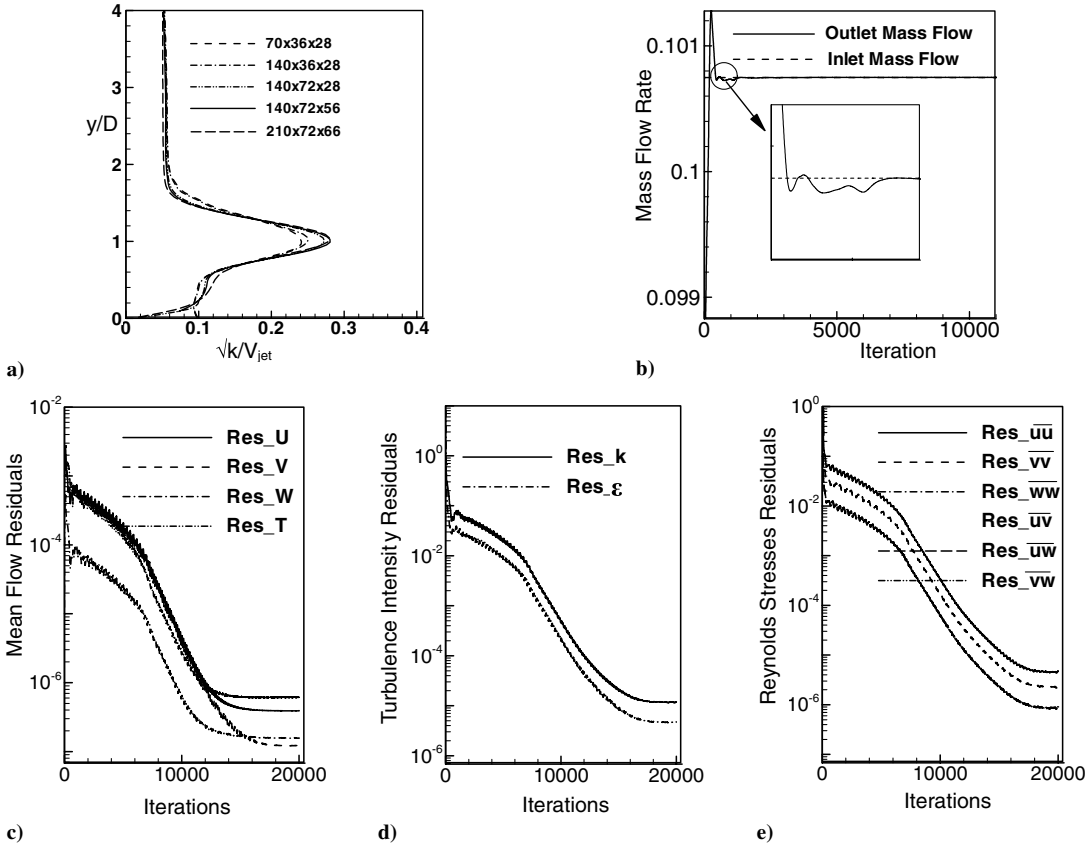

Fig. 8 Code verification a) effects of grid refinement, b) outlet mass flow rate history, and c–e) convergence history of different flow variables.

and outlet boundaries. From this figure, during the final iterations, as well as when the problem was converged, the mass is conserved properly. Also, Figs. 8c–8e show the convergence history for 1) the mean quantities, 2) the turbulence kinetic energy and its dissipation rate, and 3) Reynolds stresses, respectively. On the other hand, the results showed that at residual levels 10^{-6}–10^{-7} for turbulence intensities and 10^{-7}–10^{-8} for mean quantities the solution was not changed.

VI. Results and Discussions

In this work, we have introduced a new approach to control near-wall interactions between the jet and the crossflow to reduce flow mixing and thus improve film-cooling effectiveness. To achieve this goal, several techniques were examined, including the combination of suction/blowing jets [86–90]. Eventually, two small coolant jets were considered at both sides just downstream of the main jet forming a *combined-triple-jets unit*. For comparison purposes, in addition to the RSM, we used the SST, the k-ε, and the k-ω models for the ordinary single jet film-cooling system (as different case studies). However, as it was shown in the preceding parts of this paper, the RSM has much more capability to predict film-cooling flow physics. Thus, we used this model for our novel CTJ problem.

The new CTJ technique has four main significant effects, namely, 1) considerable mixing reduction between the coolant jets and the hot crossflow, 2) substantial film-cooling enhancement, 3) significant improvement in uniform coolant film distribution, and 4) noticeable skin friction drag reduction.

A. Reduction of Mixing Among the Coolant Jets and the Main Hot Freestream

As mentioned earlier, when a jet is injected into a crossflow, a CRVP is generated right after the jet (Fig. 9), which moves downstream in a helical fashion. This also occurs for the two new small jets in the CTJ. In other words, two weaker CRVPs are created at both sides just downstream of the main coolant jet. Note, the vortical field created by the main coolant jet and the two small jets interact, while moving in opposite directions. As shown in Fig. 9b, the right mate of the CRVP, generated by the left jet, interacts with the left mate of the CRVP, generated by the main jet, and vice versa. Notice from this figure that, in the ordinary case, the CRVP vortices have opposite signs, although they can not weaken each other (because they have the same direction at their contact points). At the contact points between the vortices of the main jet and those of the two new small jets, the vortices have opposite directions and thus weakening of their strengths occurs. Note, the interactions among the vortices, which are in opposite directions at their contact points (and thus are weakening each other), are the main key to our new approach. This leads to less interactions of the coolant jets with the hot crossflow and thus less mixing occurs among them. The reduction of this mixing strength causes considerable enhancement of the stability and the steadiness of the coolant effects downstream of the jet injections.

Figure 10 compares the mean streamwise velocity profile of CTJ with that of the regular film-cooling hole at locations $z/D = 0$ and $x/D = 3$, 5, 8, and 15. This figure demonstrates the existence of a wake region near the jets. Note, as shown in this figure, in the case of regular cooling hole 1) the wake flow is stronger, 2) the effects of the wake region far away from the jet are more clear, and 3) the mean streamwise velocity has higher gradient near the wall. These effects are not desirable from a film-cooling standpoint.

Figure 11 compares the turbulent kinetic energy profiles of the CTJ with that of the regular film-cooling hole at locations $z/D = 0$ and $x/D = 3$, 5, 8, and 15. Note from this figure that, in both cases, the peak of turbulent kinetic energy occurs at the same y/D at different streamwise positions. Also, the turbulence level near the wall for the CTJ is less than that of the ordinary one. In other words, the local near-wall turbulence generation is higher for the ordinary cooling hole. Thus, interactions between the mainstream and the coolant jets in the CTJ case are weaker, which is useful from a cooling performance point of view.

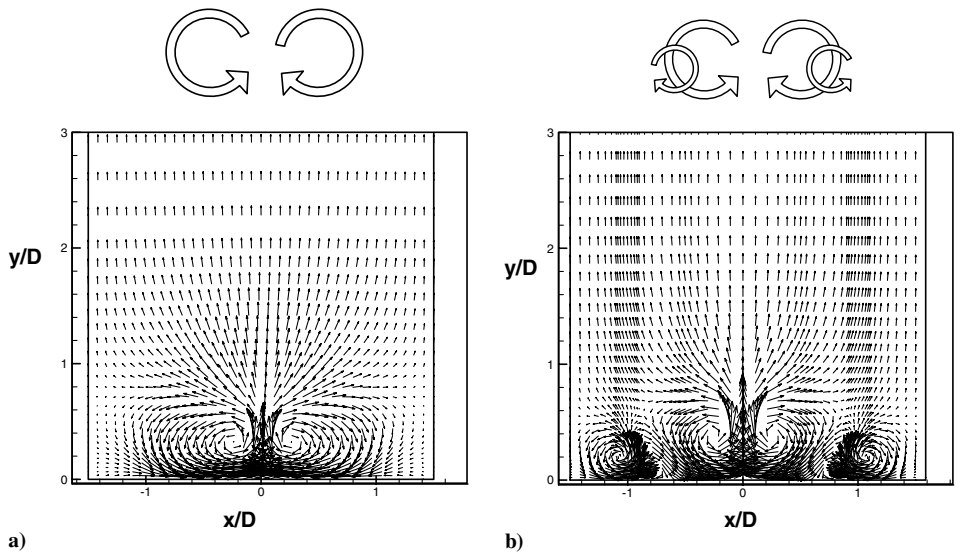

Fig. 9 CRVPs mechanism at $x/D = 2$ a) ordinary film cooling and b) CTJ.

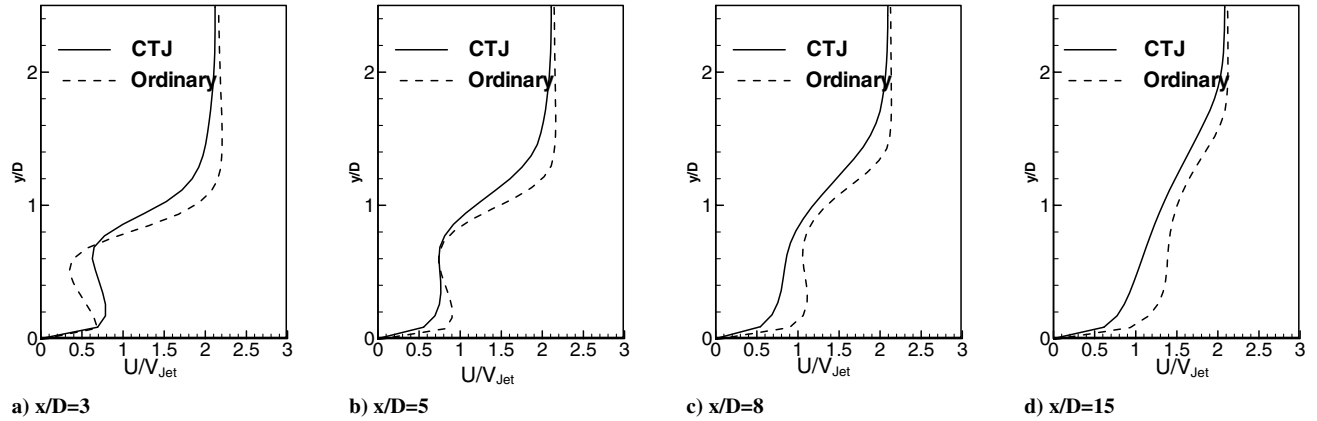

Fig. 10 Comparison of the mean streamwise velocity profiles of CTJ and ordinary film cooling at different locations.

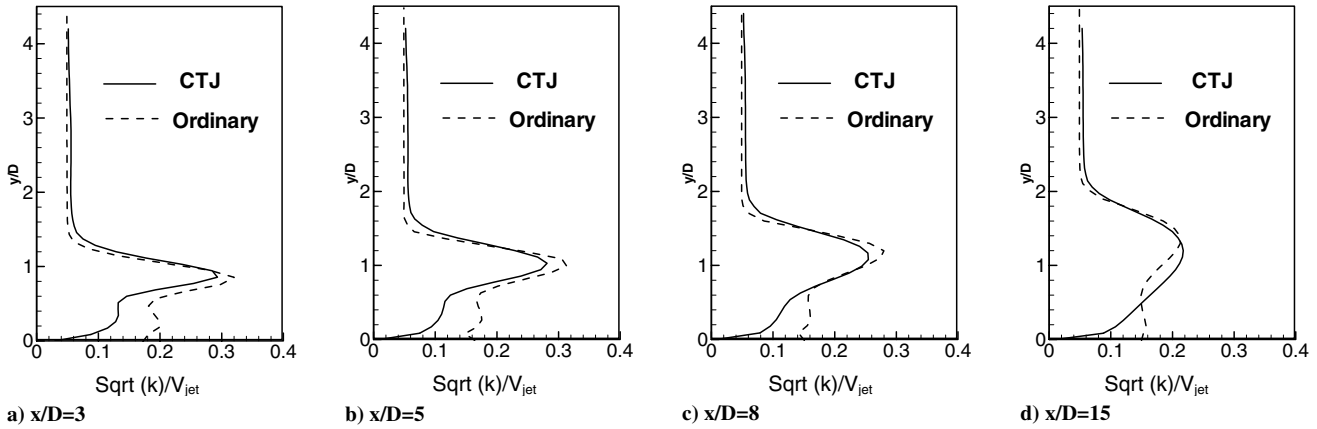

Fig. 11 Comparison of the turbulent kinetic energy profiles in CTJ and in ordinary film cooling at different locations.

B. Considerable Improvement of Film-Cooling Effectiveness

The injection of the coolant jets into the crossflow makes a low-pressure region just behind the jets, causing the hot gases to flow into this region, producing a layer of hot gases beneath the coolant jets, and thus reducing the film-cooling effectiveness.

Figure 12 shows this schematically (top) and numerically (bottom). The main goal of our new approach is to avoid the flow of these hot gases into this low-pressure region. We examined several techniques [86–90] and finally reached the most efficient one (CTJ). Figure 12b shows how the new small jets divert the hot gases from flowing beneath the coolant jets. In this situation, the coolant jets fill in the low-pressure region, instead of the hot gases.

Also, note from Fig. 13a that during the rotation of the CRVP generated by the main coolant jet (in ordinary film cooling), the hot gases come down toward the surface continuously and do not permit the coolant film to cool down surfaces well enough. Whereas, in our new technique, like a fluid barrier, the interactions between the vortical fields generated by the main and the small jets prevent the

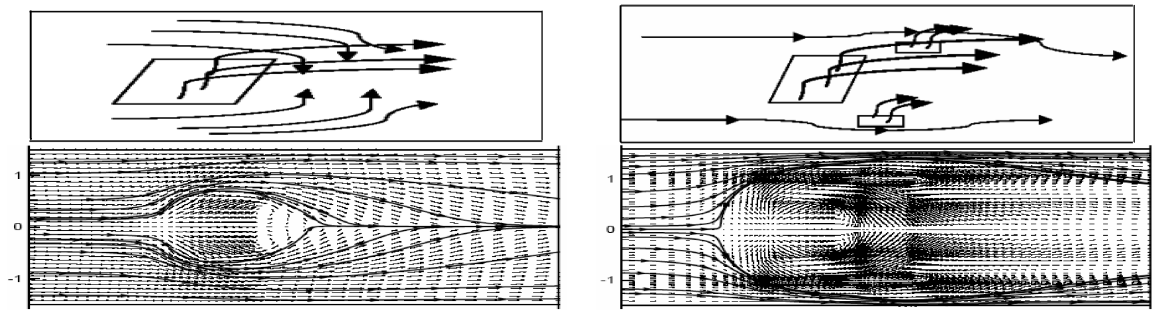

Fig. 12 The streamline passing around the cooling holes near the wall a) ordinary holes, and b) CTJ.

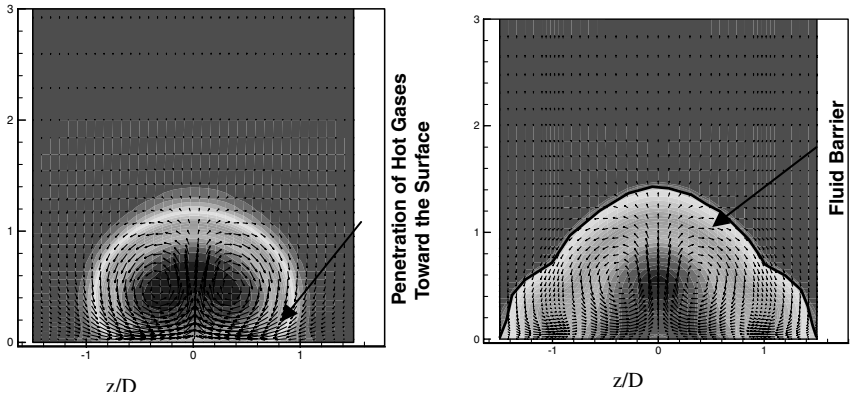

a) **b)**

Fig. 13 CRVPs superimposed with temperature field at $x/D = 5$ a) ordinary film cooling and b) CTJ.

penetration of the hot gases toward the surface (Fig. 13b). Also, the penetration of the jets into the crossflow boundary layer is less in our new approach (compared to that of the ordinary one), which is important from a film-cooling viewpoint.

Figure 14 shows the local temperature distribution at different locations $x/D = 3$, 5, 8, and 15 downstream of the coolant jets for both the ordinary and the CTJ film-cooling systems. This figure illustrates that the spanwise spreading of the coolant film in the CTJ

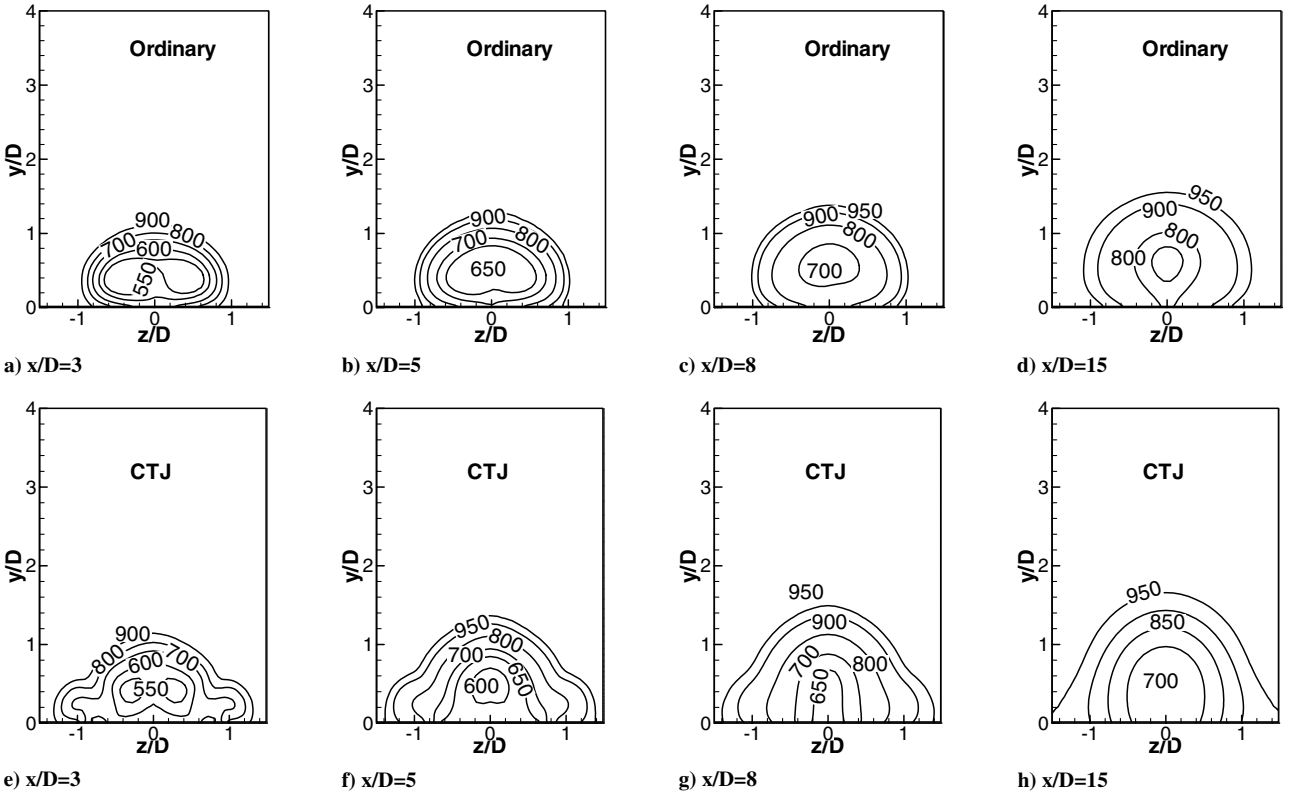

a) x/D=3 **b) x/D=5** **c) x/D=8** **d) x/D=15**

e) x/D=3 **f) x/D=5** **g) x/D=8** **h) x/D=15**

Fig. 14 Contour plots of local temperature distribution at different x/D positions a–d) ordinary film cooling and e–h) CTJ.

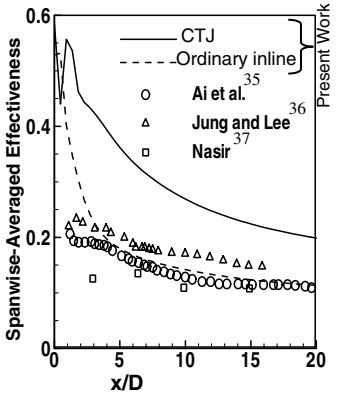

Fig. 15 Comparison of our ordinary and CTJ (both in-line) spanwise-averaged film-cooling effectiveness with experimental works (in-line).

case is higher, resulting in a more uniform coolant film distribution and film-cooling effectiveness. Also, note from this figure that in the ordinary film cooling, as the flow moves further downstream from the jet exit, the coolant film moves away from the surface and thus its cooling effectiveness decreases. However, in the CTJ technique, the coolant film stays very close to the surface all the way through.

Figure 15 compares the spanwise-averaged film-cooling effectiveness of our new approach and that of the ordinary film cooling, showing a considerable improvement (about 50%) when the new approach is used. Some related experimental results of the ordinary film cooling [35–37] are also shown in this figure (their jet exit geometry are somewhat different). As shown in this figure, the CTJ case has the highest film-cooling effectiveness.

C. Significant Improvement in Uniform Film-Cooling Distribution

Having more uniform coolant film distribution is also very important in the film-cooling problem. One of the advantages of the staggered rows (compared with in-line rows) is that, for the same hole geometry and flow characteristics, the total uniformity of the staggered holes is higher (because the jets' flow overlaps). The existence of two small coolant jets at both sides downstream of the main jet, which makes a CTJ unit (with respect to one unit of ordinary film cooling: in-line or staggered), leads to even more uniform coolant film distribution. Also, because of less interactions between the crossflow and the coolant jets, less penetration into the hot crossflow boundary layer, and more coolant film spreading in spanwise direction, in our novel CTJ unit, this uniformity continues in the regions much further downstream of the jet. Comparison of the spanwise-averaged and the centerline film-cooling distribution can be considered as a criterion for the uniformity of the coolant film distribution. In other words, in a well-distributed coolant film, the spanwise-averaged film-cooling effectiveness distribution is closer to the centerline one. Figures 16a and 16b show this matter for the ordinary and for the CTJ film-cooling cases, respectively. As shown in this figure, the spanwise-averaged film-cooling effectiveness in the CTJ problem is closer to its centerline value and thus has more uniform film cooling.

D. Enhancement of Skin Friction Drag Reduction

Although many studies have been performed on jet-into-crossflow problems, only a few people have studied its effects on surface friction drag. In our study, we have compared this coefficient where using the new approach with that of the ordinary one (assuming a smooth wall [90]). Because the skin friction drag is directly related to the shear stresses at the wall (and thus to the velocity gradients there), we need to look at the wall velocity gradients with and without the coolant jets. Because the velocity at the wall is zero, the velocity at the first cell right above the wall divided by its distance from the wall gives a close approximation for the velocity gradient there (because we used a structured grid, all such distances are equal). Using this analysis, the distribution of the velocity gradient along the wall can be easily investigated.

As our results show, when a jet is injected into a crossflow, the skin friction drag is decreased. This is because the velocity profiles are disturbed by the coolant jet near the wall. The new profiles have less gradients at the wall (particularly at locations near the jet injection). However, as the flow moves downstream, the effects of the coolant jets decrease and the flow tends to have a regular profile. Therefore, we expect an increase in skin friction drag farther downstream of the jet exit. The more the turbulent boundary layer gets distorted and the more this distortion continues downstream, the more reduction in the skin friction drag is expected (see also Fig. 10). Figure 17 compares the skin friction drag coefficient (spanwise-averaged) along the streamwise direction. For comparison purposes, the skin friction drag coefficient of a fully developed turbulent flow over a flat plate without any jet injection is also shown in this figure. As noted, the skin friction drag coefficient for turbulent flow without jet injection is higher. Also, the skin friction drag coefficient in our new approach is about 20% less than that of the ordinary one (see [90] for more details).

E. CTJ Versus Double Rows Staggered Cooling Holes Arrangement

We should emphasize here that our new technique is different from the regular double rows staggered holes arrangement, which is widely used in film-cooling applications. The main goal of the staggered rows is to improve film-cooling effectiveness by overlapping the coolant jets which improves the uniformity of the coolant-film distribution (not necessarily the reduction of hot and cold mixing interactions). In other words, there are not very strong interactions between the neighboring vortices in the regular

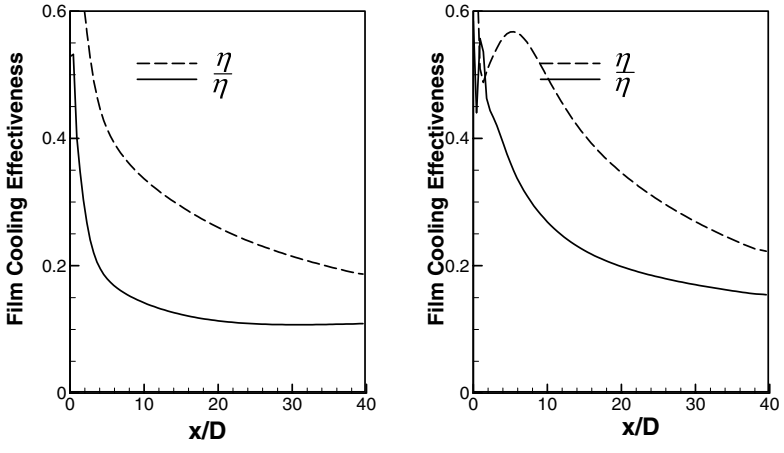

Fig. 16 Comparison of the spanwise-averaged and the centerline film-cooling effectiveness a) ordinary film cooling and b) CTJ.

Table 4 Some of the previous studies on staggered film-cooling holes

Case	Year	Hole pitch ratio, P/D	Row spacing ratio, S/D	Inclination angle	Blowing ratio
Miao et al. [59,60]	2006-2006	3	3	35	0.3–1.5
Ahn et al. [61]	2006	5.97	3.4	30	0.5–2.0
Saumweber [62]	2006	4	10, 20, 30	30	0.5–2.0
Yuen et al. [63,64]	2005-2005	6	12.5	30, 60, 90	0.33–2.0
Ahn et al. [28]	2003	6	4	35	0.5–2.0
Petre et al. [65]	2003	6	6	90	1.0–5.0
Ligrani and Lee [54]	2003	6	4	24	0.5–4.0
Ligrani and Ramsey [53]	1997	6	4	30	0.5–1.5
Martiny et al. [66]	1995	4.5	7.6	17	0.5–4.0
Andrews et al. [67]	1995	11	11	30, 150	1.0–14.0
Amer et al. [68]	1992	3	10	30	0.2–1.0
Jubran [69]	1989	3	10	30, 90	0.2–1.0
Sasaki et al. [70]	1979	3	5, 10	45	0.15–0.5
Mayle and Camarata [71]	1975	8, 10, 14	6.9, 8.7, 12.1	30	.25–2.0

staggered cooling holes arrangement (detailed discussions are made in the proceeding).

In this section, the CTJ and the double rows staggered jets arrangements are compared and discussed in detail. Depending on different flow and geometrical parameters, there are numerous choices to arrange the locations of the staggered jets in a film-cooling system. Some of the previous investigations of staggered jets film cooling are summarized in Table 4. Also, Fig. 18 shows a typical arrangement of a system of staggered jets arrangement.

Among various film-cooling jet arrangements, we considered the two cases studied by Ligrani et al. [52–55] (experimental) and Miao and Wu [60] (numerical). For the former, the freestream velocity was 10 m/s (ours was 11 m/s) and the hole diameter was 9.25 mm (ours was 12.7 mm). Whereas, for the latter case, the freestream velocity was 10 m/s and the hole diameter was 5 mm (employing k-ε turbulence model). Because our computer code uses a Cartesian coordinate system and most of the previous works have used cylindrical holes, it is not possible to have very quantitative comparisons.

Figure 19 compares the CTJ cooling performance with that of the ordinary (both in-line and staggered) film-cooling systems. This figure shows that the ordinary staggered film-cooling system has higher cooling effectiveness than that of the in-line ordinary one. However, the in-line CTJ arrangement has higher cooling effectiveness than that of the staggered arrangement, whereas the staggered arranging of CTJ has higher cooling effectiveness than that of the ordinary staggered film cooling. The experimental results of Ligrani et al. [54] are also shown in this figure for a staggered arrangement ($p/D = 6$ and $s/D = 4$). These results and the results of our numerical simulation for the ordinary staggered arrangement of the coolant jets are relatively close and both show similar trends for film-cooling effectiveness. The differences between the two results are mainly due to the fact that the two cases use different jet hole geometries. One can also note from this figure that our in-line CTJ case has the highest cooling effectiveness among the staggered CTJ and the in-line/staggered arrangements of the ordinary film cooling systems.

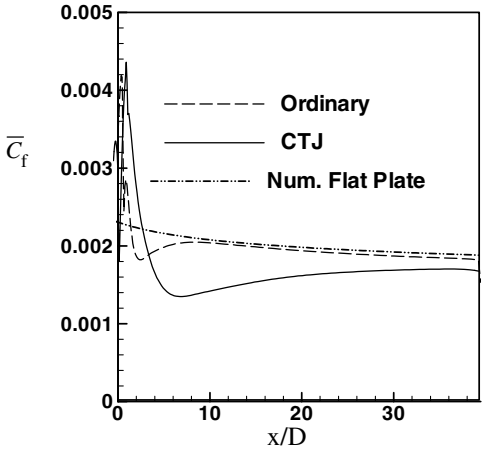

Fig. 17 Comparison of the spanwise-averaged skin friction drag coefficient for CTJ and for ordinary film cooling.

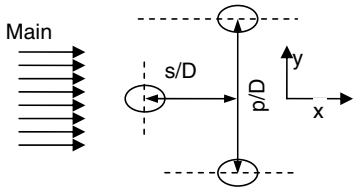

Fig. 18 Typical arrangement of regular staggered film-cooling jets.

Figure 20 compares the spanwise-averaged film-cooling effectiveness distribution of the staggered arrangement of the novel CTJ with the numerical simulation of Miao and Wu [60], who used a staggered arrangement of different hole geometries ($p/D = 3$ and $s/D = 3$), namely, 1) cylindrical round, simple angle (CYSA), 2) forward-diffused simple angle (FDSA), and 3) laterally diffused, simple angle (LDSA). Note, their lateral direction is equivalent to our spanwise one. This figure shows that our CTJ has higher cooling performance relative to the cases studied by Miao and Wu [60].

Figures 21a–21f show the film-cooling effectiveness contour for the 1) in-line arrangement of the ordinary film cooling, 2) staggered arrangements of the ordinary film cooling ($p/D = 6$ and $s/D = 4$), 3) LDSA results of Miao and Wu [60] ($p/D = 3$ and $s/D = 3$), 4) in-line arrangements of the CTJ, 5) staggered arrangements of the CTJ ($p/D = 6$ and $s/D = 4$), and 6) staggered arrangements of the CTJ ($p/D = 3$ and $s/D = 3$), respectively. Note, the dashed lines in these figures mean that these regions are not solved in our simulation;

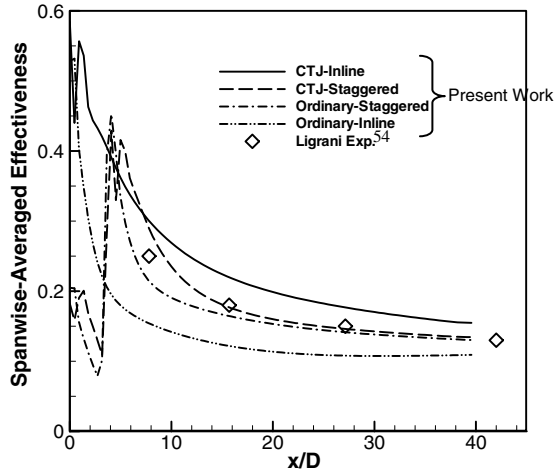

Fig. 19 Spanwise-averaged film-cooling effectiveness for different cooling holes arrangement.

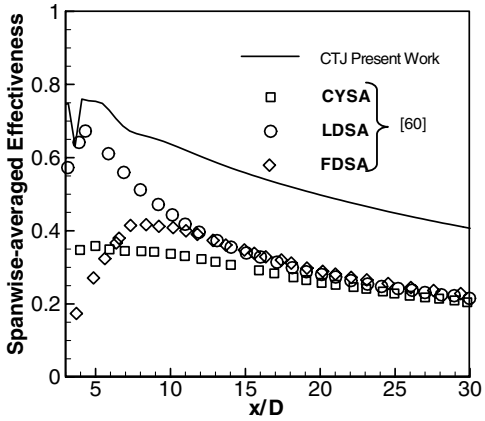

Fig. 20 Spanwise-averaged film-cooling effectiveness of CTJ in staggered arrangement.

however, they have been considered by imposing periodic or symmetric boundary conditions in the spanwise direction. As shown in this figure, the CTJ cooling holes (right) have higher performance with respect to their corresponding ordinary cooling holes (left), particularly in the region downstream of the jets in both staggered and in-line arrangements. Comparing Figs. 21c and 21f emphasizes that our simple geometry of CTJ has higher cooling effectiveness, compared with the complex hole shapes film-cooling system of Miao and Wu [60].

Finally, Figs. 22a and 22b compare the spanwise-averaged and the centerline film-cooling effectiveness (the criterion for uniform film-cooling distribution) for two different staggered arrangements ($p/D = 6$ with $s/D = 4$ and $p/D = 3$ with $s/D = 3$), respectively. As shown in this figure, the latter case has an excellent film-cooling uniformity.

Note, this work is a fundamental study in introducing a new approach to control the mixing in jet-into-crossflow problems,

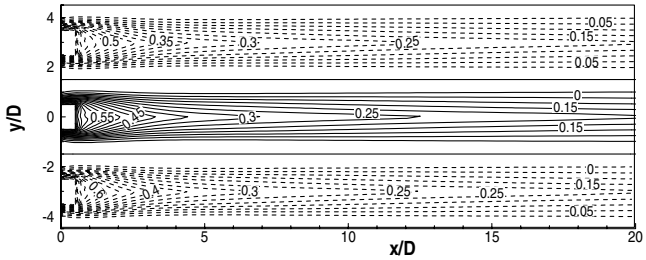

a) Inline ordinary (present work)

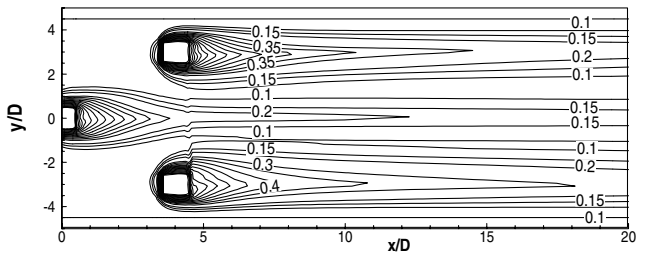

b) Staggered ordinary, p/D=6 and s/D=4 (present work)

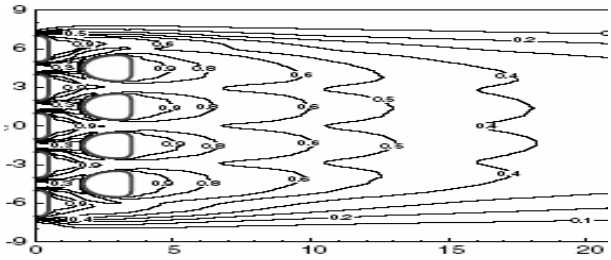

c) Ordinary staggered, p/D=3 and s/D=3, (Miao[60])

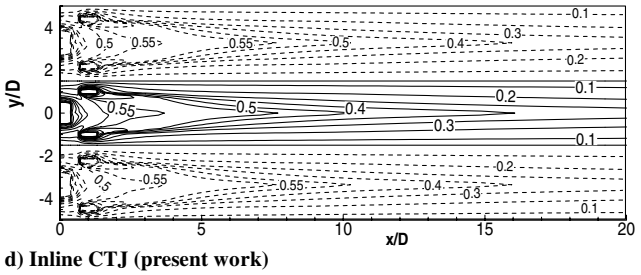

d) Inline CTJ (present work)

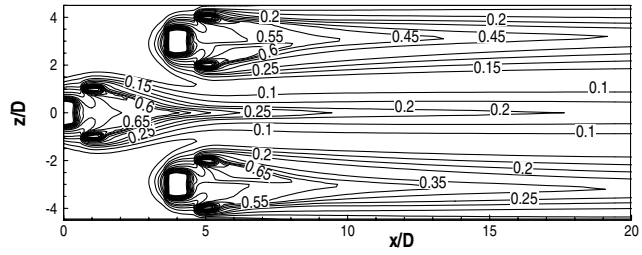

e) Staggered CTJ, p/D=6 and s/D=4 (present work)

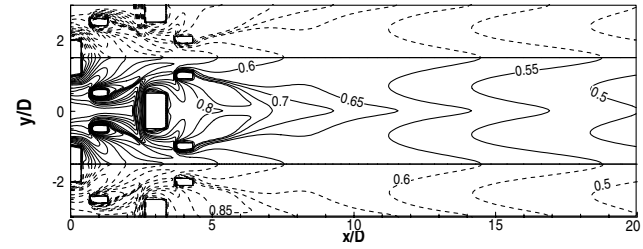

f) Staggered CTJ, p/D=3 and s/D=3 (present work)

Fig. 21 Comparison of local film cooling effectiveness contours, a–c) the ordinary film cooling, and d–f) the CTJ, at different arrangements.

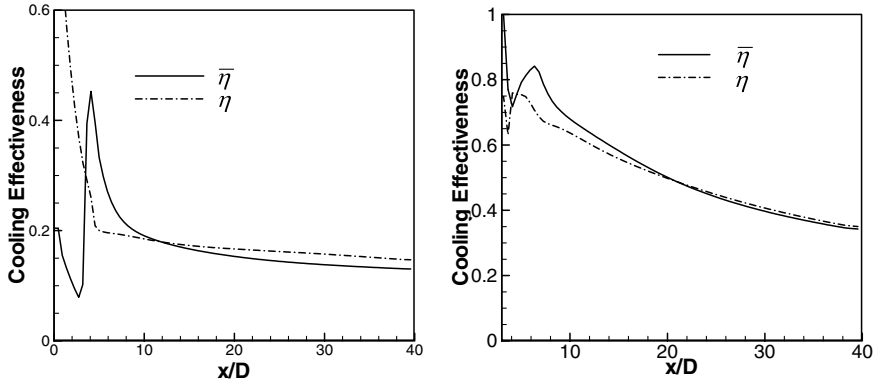

a) p/D=6, s/D=4 **b) p/D=3, s/D=3**

Fig. 22 Comparison of the spanwise-averaged and the centerline film-cooling effectiveness for staggered CTJ at two different arrangements.

particularly that it improves the film-cooling effectiveness. Of course, more work needs to be done to optimize it, and our research team is presently examining the effects of different jet geometries and flow characteristics.

VII. Conclusions

In this work, we introduced a novel near-wall flow control technique of using a staggered arrangement of small injection ports near a film-cooling hole to improve film-cooling effectiveness and to have a more uniform film-cooling distribution. Our computational results showed that these two small jets changed the flow pattern drastically and thus reduced the mixing between the coolant jets and the main hot freestream.

The most important advantages of using the CTJ cooling system are summarized here. First of all, the mixing between the hot crossflow and the coolant jets was considerably reduced, which increased the stability and the steadiness of the coolant effects downstream of the injection. Secondly, the overall film-cooling effectiveness was significantly improved, i.e., for the same hole cross section and for the same total injection mass flow rate, the CTJ showed at least 50% higher film-cooling effectiveness in in-line arrangement. Thirdly, a much more uniform film-cooling distribution was obtained, i.e., a closer spanwise-averaged to centerline film-cooling effectiveness was achieved, resulting in a more uniform coolant-film distribution. Also, the skin friction drag was considerably reduced, i.e., the spanwise boundary layer was disturbed much more and for longer streamwise distances, leading to about 20% reduction in skin friction drag. Finally, the novel CTJ results showed considerable improvement compared with the regular double rows staggered hole arrangement.

These advantages were obtained through prevention of hot crossflow penetration beneath the coolant jets, weakening of the strength of the CRVP, lessening of the coolant-film penetration into the hot crossflow boundary layer, and suitably spreading of the coolant film in the spanwise direction.

References

[1] Margason, R. J., *Fifty Years of Jet in Cross Flow Research*, AGARD, CP-534, 1993.

[2] Darbandi, M., Taiebi-Rahni, M., Schneider, G. E., Javadi, K., and Javadi, A., "Numerical Prediction on the Interaction of a Jet and a Turbulent Boundary Layer," *The 33rd AIAA Fluid Dynamics Conference*, AIAA, Paper No. 3730-2003, 2003.

[3] Andreopoulos, J., and Rodi, W., "Experimental Investigation of Jets in a Crossflow," *Journal of Fluid Mechanics*, Vol. 138, June 1984, pp. 93–127.

[4] Haven, B. A., and Kurosaka, M., "Kidney and Anti-Kidney Vortices in Crossflow Jets," *Journal of Fluid Mechanics*, Vol. 352, Dec. 1997, pp. 27–64.

[5] Feric, T. F., "Structure of Near Field of the Transverse Jet," Ph.D. Dissertation, Mechanical Engineering Dept., California Univ. of Technology, Pasadena, CA, 1990.

[6] Kim, S. W., and Benson, T. J., "Fluid Flow of a Row of Jets in Crossflow: A Numerical Study," *AIAA Journal*, Vol. 31, No. 5, 1993, pp. 806–811.

[7] Schaeffler, N. W., "The Interaction of a Synthetic Jet and a Turbulent Boundary Layer," *41st Aerospace Science Meeting & Exhibition*, AIAA Paper 0643, 2003.

[8] Pope, S. B., *Turbulent Flows*, Cambridge Univ. Press, London, 2000.

[9] Ajersch, P., Zhou, J. M., Ketler, S., Salcudean, M., and Gartshore, I. S., "Multiple Jets in a Crossflow: Detailed Measurements and Numerical Simulations," ASME 95-GT-9, 1995, pp. 1–16.

[10] Hoda, A., and Acharrya, S., "Prediction of a Film Cooling Jet in Cross-Flow With Different Turbulence Models," *Journal of Turbomachinery*, Vol. 122, No. 3, July 2000, pp. 558–569.

[11] Amer, A. A., Jubran, B. A., and Hamdan, M. A., "Comparison of Different Two-Equation Turbulence Models for Prediction of Film Cooling from Two Rows of Holes," *Numerical Heat Transfer, Part A, Applications*, Vol. 21, No. 2, 1992, pp. 143–163.

[12] Hassan, I., Findlay, M., Salcudean, M., and Gartshore, I., "Prediction of Film Cooling with Compound- Angle Injection Using Different Turbulence Models," *The Sixth Conference of the CFD Society of Canada, Proceedings of CFD98*, Quebec, Canada, 1998, pp. 416–424.

[13] Medic, G., and Durbin, P., "Toward Improved Prediction of Heat Transfer on Turbine Blades," *Journal of Turbomachinery*, Vol. 124, No. 2, April 2002, pp. 187–191.

[14] Medic, G., and Durbin, P., "Toward Improved Film Cooling Prediction," *Journal of Turbomachinery*, Vol. 124, No. 2, April 2002, pp. 193–199.

[15] Keimasi, M. R., and Taeibi-Rahni, M., "Numerical Simulation of Jets in a Cross Flow Using Different Turbulence Models," *AIAA Journal*, Vol. 39, No. 12, 2001, pp. 2268–2277.

[16] Javadi, A., Javadi, K., Taeibi-Rahni, M., and Keimasi, M., "Reynolds Stress Turbulence Models for Prediction of Shear Stress Terms in Cross Flow Film Cooling Numerical Simulation," *Proceedings of Computational Technologies for Fluid/Thermal/Structural/Chemical Systems with Industrial Applications*, Vol. 2, edited by C. R. Kleijn, S. Kawano, V. V. Kudriavtsev, American Society of Mechanical Engineers, New York, 2002.

[17] Thevenin, J., Amaral, M., Malvos, H., and Mauillon, L., "Computation of a Three-Dimensional Swirling Jet into a Crossflow, Using a Reynolds Stress Turbulence Model," European Community on Computational Methods in Applied Sciences Paper 98, 1998.

[18] Fu, S., Launder, B. E., and Leschziner, M. A., "Modeling Strongly Swirling Recirculating Jet Flow with Reynolds-Stress Transport Closures," *Proceeding of the Sixth Symposium on Turbulent Shear Flow*, Vol. 6, Pennsylvania State Univ., University Park, PA, 1987, pp. 17.6.1–17.6-6.

[19] Ince, N. Z., and Leschziner, M. A., "Calculation of Single and Multiple Jets in Cross Flow with and Without Impingement Using Second-Moment Closure," *Engineering Turbulence Modelling and Experiments*, Elsevier, New York, 1990, pp. 155–164.

[20] Tyagi, M., and Acharya, S., "Large Eddy Simulation of Jets in Crossflow: Free Stream Turbulence Effects," *The 3rd ASME/JSME Joint Fluid Engineering Conference*, Fluids Engineering Division Summer Meeting Paper 99-7799, 1999.

[21] Ramezani-Zadeh, M., and Taeibi-Rahni, M., "Large Eddy Simulation of Multiple Jets in a Cross Flow Using Smagorinsky Model," *ISME 2001*, Guilan Univ., Rasht, Iran, 2001, pp. 293–299.

[22] Ramezani-Zadeh, M., Saidi, M. H., and Taeibi-Rahni, M., "Large Eddy Simulation of Density Ratio Effects on Two-Dimensional Film Cooling," *Proceedings of the 2nd BSME-ASME International Conference on Thermal Engineering*, Vol. 2, American Society of Mechanical Engineers, New York, 2004, pp. 659–665.

[23] Eckert, E. R. G., and Livingood, J. N. B., "Comparison of Effectiveness of Convection, Transpiration, and Film-Cooling Methods with Air as Coolant," NASA Rept.-1182, 1954.

[24] Bladauf, S., Schulz, A., and Witting, S., "High-Resolution Measurements of Local Heat Transfer Coefficients from Discrete Hole Film Cooling," *Journal of Turbomachinery*, Vol. 123, No. 4, 2001, pp. 749–757.

[25] Goldstein, R. J., Jin, P., and Olson, R. L., "Film Cooling Effectiveness and Mass/Heat Transfer Coefficient Downstream of One Row of Discrete Holes," *Journal of Turbomachinery*, Vol. 121, No. 4, 1999, pp. 225–232.

[26] Bell, C. M., Hamakawa, H., and Ligrani, P. M., "Film Cooling From Shaped Holes," *Journal of Heat Transfer*, Vol. 122, No. 2, 2000, pp. 224–232.

[27] Sinha, A. K., Bogard, D. G., Crawford, M. E., "Film Cooling Effectiveness Downstream of a Single Row of Holes with Variable Density Ratio," *ASME, International Gas Turbine and Aeroengine Congress and Exposition, The 35th*, Allied-Signal Aerospace Co., Columbia, MD, 1990, p. 9.

[28] Ahn, J., Jung, I. S., and Lee, J. S., "Film Cooling from Two Rows of Holes with Opposite Orientation Angle: Injectant Behavior and Adiabatic Film Cooling Effectiveness," *International Journal of Heat and Fluid Flow*, Vol. 24, No. 1, Feb. 2003, pp. 91–99.

[29] Chang, Y. R., and Chen, K. S., "Prediction of Opposing Turbulent Line Jets Discharged Laterally into Confined Crossflow," *International Journal of Heat and Mass Transfer*, Vol. 38, No. 9, 1995, pp. 1693–1703.

[30] Bridges, A., and Smith, D. R., "Influence of Orifice Orientation on the Synthetic Jet-boundary-layer Interaction," *AIAA Journal*, Vol. 41, No. 12, 2003, pp. 2349–2402.

[31] McGrath, L. E., and Leylek, J. H., "Physics of Hot Crossflow Ingestion in Film Cooling," *Journal of Turbomachinery*, Vol. 121, No. 3, 1999, pp. 532–541.

[32] Goldstein, R. J., and Stone, L. D., "Row-of-Holes Film Cooling of Curved Walls at Low Injection Angle," *Transactions of ASME, Series G: Journal of Dynamic Systems, Measurement and Control*, Vol. 119, No. 3, July 1997, pp. 574–579.

[33] Azzi, A., Abidat, M., Jubran, B. A., and Theodoridis, G. S., "Film Cooling Predictions of Simple and Compound Angle Injection from One and Two Staggered Rows," *Numerical Heat Transfer, Part A, Applications*, Vol. 40, No. 3, 2001, pp. 273–294.

[34] Jubran, B. A., and Maiteh, B. Y., "Film Cooling and Heat Transfer from a Combination of Two Rows of Simple and/or Compound Angle Holes in Inline and/or Staggered Configurations," *International Journal of Heat and Mass Transfer*, Vol. 34, No. 6, 1999, pp. 495–502.

[35] Ai, D., Ding, P. P., and Chen, P. H., "The Selection Criterion of Injection Temperature Pair for Transient Liquid Crystal," *International Journal of Heat and Mass Transfer*, Vol. 44, No. 7, 2001, pp. 1389–1399.

[36] Jung, I. S., Lee, J. S., "Effects of Orientation Angles on Film Cooling over a Flat Plate: Boundary Layer Temperature Distributions and Adiabatic Film Cooling Effectiveness," *Journal of Turbomachinery*, Vol. 122, No. 1, 2000, pp. 153–160.

[37] Nasir, H., Ekkad, S. V., and Acharya, S., "Effect of Compound Angle Injection on Flat Surface Film Cooling with Large Streamwise Injection Angle," *Experimental Thermal and Fluid Science*, Vol. 2, No. 2, Aug. 2001, pp. 23–29.

[38] Gartshore, I., and Salcudean, M., "*Film Cooling Injection Hole Geometry: Hole Shape Comparison for Compound Cooling Orientation*," *AIAA Journal*, Vol. 39, No. 8, 2001, pp. 1493–1499.

[39] Mahjoob, Sh., and Taeibi-Rahni, M., "Parameter Affecting Turbulent Film Cooling, Reynolds-Averaged Navier–Stokes Computational Simulation," *Journal of Thermophysics and Heat Transfer*, Vol. 20, No. 1, 2006, pp. 92–100.

[40] Rowbury, D. A., Oldfield, M. L. G., and Lock, G. D., "A Method for Correlating the Influence of External Crossflow on the Discharge Coefficient of Film Cooling Holes," *Journal of Turbomachinery*, Vol. 123, No. 2, 2001, pp. 258–265.

[41] Holdeman, J. D., and Walker, R. E., "Mixing of a Row of Jets with a Confined Crossflow," *AIAA Journal*, Vol. 15, No. 2, 1977, pp. 243–249.

[42] Teng, S., and Han, Je-C., "Effect of Film-Hole Shape on Turbine-Blade Heat-Transfer Coefficient Distribution," *Journal of Thermophysics and Heat Transfer*, Vol. 15, No. 3, 2001, pp. 249–256.

[43] Cutbirth, J. M., and Bogard, D. G., "Evaluation of Pressure Side Film Cooling with Flow and Thermal Field Measurements, Part 1: Showerhead Effects," *Journal of Turbomachinery*, Vol. 124, No. 4, 2002, pp. 670–677.

[44] Goldstein, R. J., Eckert, E. R. G., and Burggraf, F., "Effects of Hole Geometry and Density on Three-Dimensional Film Cooling," *International Journal of Heat and Mass Transfer*, Vol. 17, No. 5, 1973, pp. 595–607.

[45] Hyung, H. C., Seung, G. K., and Dong, H. R., "Heat/Mass Transfer Measurement Within a Film Cooling Hole of Square and Rectangular Cross Section," *ASME Transactions: Journal of Tribology*, Vol. 123, No. 4, 2001, pp. 806–814.

[46] Friedrichs, S., Hodson, H. P., and Dawes, W. N., "The Design of an Improved End Wall Film-Cooling Configuration," *Journal of Turbomachinery*, Vol. 121, No. 4, 1999, pp. 772–780.

[47] Burd, S. W., Kaszeta, R. W., and Simon, T. W., "Measurements in Film Cooling Flows: Hole L/D and Turbulence Intensity," *Journal of Turbomachinery*, Vol. 120, No. 4, 1998, pp. 791–798.

[48] Walters, D. K., and Leylek, J. H., "A Systematic Computational Methodology Applied to a Three-Dimensional Film Cooling Flowfield," *Journal of Turbomachinery*, Vol. 119, No. 4, 1997, pp. 777–785.

[49] Seo, H. J., Lee, J. S., and Ligrani, P. M., "The Effect of Injection Hole Length on Film Cooling with Bulk Flow Pulsations," *International Journal of Heat and Mass Transfer*, Vol. 41, No. 22, 1998, pp. 3515–3528.

[50] Plesniak, M. W., "Noncanonical Short Hole Jet-in-Crossflow for Turbine Film Cooling," *Journal of Applied Mechanics*, Vol. 73, No. 3, 2006, pp. 747–482.

[51] Azzi, A., and Jubran, B. A., "Numerical Modeling of Film Cooling from Short Length Stream-Wise Injection Holes," *International Journal of Heat and Mass Transfer*, Vol. 39, No. 4, 2003, pp. 345–353.

[52] Ligrani, P. M., Ciriello, S., and Bishop. D. T., "Heat Transfer, Adiabatic Effectiveness, and Injectant Distributions Downstream of a Single Row and Two Staggered Rows of Compound Angle Film Cooling Holes," *Journal of Turbomachinery*, Vol. 114, No. 4, 1992, pp. 687–700.

[53] Ligrani, P. M., Wigle, J. M., Ciriello, S., and Jackson, S. W., "Film-Cooling from Holes with Compound Angle Orientations, Part 1: Results Downstream of Two Staggered Rows of Holes with 3D Spanwise Spacing," *Journal of Heat Transfer*, Vol. 116, No. 2, 1994, pp. 341–352.

[54] Ligrani, P. M., and Ramsey, A. E., "Film Cooling from Spanwise-Oriented Holes in Two Staggered Rows," *Journal of Turbomachinery*, Vol. 119, No. 3, 1997, pp. 562–567.

[55] Ligrani, P. M., and Lee, J. S., "Film Cooling from Two Staggered Rows of Compound Angle Holes at High Blowing Ratio," *International Journal of Rotating Machinery*, Vol. 2, No. 3, 2003, pp. 201–208.

[56] Dittmar, J., Schulz, A., and Wittig, S., "Adiabatic Effectiveness and Heat Transfer Coefficient of Shaped Film Cooling Holes on a Scaled Guide Vane Pressure Side Model," *International Journal of Rotating Machinery*, Vol. 10, No. 5, 2004, pp. 345–354.

[57] Behbahani, A. I., and Goldstein, R. J., "Local Heat Transfer to Staggered Arrays of Impinging Circular Air Jets," *Journal of Engineering for Power*, Vol. 105, No. 5, 1983, pp. 354–360.

[58] Garg, V. K., "Heat Transfer on a Film-Cooled Rotating Blade," NASA Paper CR-1999-209301, 1999.

[59] Ekkad, S. V., Gao, L., and Hebert, R. T., "Effect of Jet-to-Jet Spacing in Impingement Arrays on Heat Transfer," American Society of Mechanical Engineers Paper IMECE2002-32108, 2002.

[60] Miao, J. M., and Wu, C. Y., "Numerical Approach to Hole Shape Effect on Film Cooling Effectiveness over Flat Plate Including Internal Impingement Cooling Chamber," *International Journal of Heat and Mass Transfer*, Vol. 49, 2006, pp. 919–938.

[61] Miao, J. M., and Ching, H. K., "Numerical Simulation of Film-Cooling Concave Plate as Coolant Jet Passes Through Two Rows of Holes with Various Orientations of Coolant Flow," *International Journal of Heat and Mass Transfer*, Vol. 49, Nos. 3–4, 2006, pp. 557–574.

[62] Ahn, J., Schobeiri, M. T., Han, J. C., and Moon, H. K., "Film Cooling Effectiveness on the Leading Region of a Rotating Turbine Blade with Two Rows of Film Cooling Holes Using Pressure Sensitive Paint," *Journal of Heat Transfer*, Vol. 128, Nos. 5–6, March 2006, pp. 879–888.

[63] Saumweber, C., "Interaction of Film Cooling Rows: Effects of Hole Geometry and Row Spacing on the Cooling Performance Downstream of the Second Row of Holes," *Journal of Turbomachinery*, Vol. 126, No. 9, 2006, pp. 237–246.

[64] Yuen, C. H. N., and Martinez-Botas, R. F., "Film Cooling Characteristics of Rows of Round Holes at Various Streamwise Angles in a Crossflow, Part 1: Effectiveness," *International Journal of Heat and Mass Transfer*, Vol. 48, Nos. 23–24, 2005, pp. 4995–5016.

[65] Yuen, C. H. N., and Martinez-Botas, R. F., "Film Cooling Characteristics of Rows of Round Holes at Various Streamwise Angles in a Crossflow, Part 2: Heat Transfer Coefficients," *International Journal of Heat and Mass Transfer*, Vol. 48, Nos. 23–24, 2005, pp. 5017–5035.

[66] Petre, B., Dorignac, E., and Vullierme, J. J., "Study of the Influence of the Number of Holes Rows on the Convective Heat Transfer in the Case of Full Coverage Film Cooling" (in French "Etude de l'Influence du Nombre de Rangées de Trous sur les Échanges Convectifs dans le cas du Refroidissement par Multiperforation"), *International Journal of Heat and Mass Transfer*, Vol. 46, Nos. 23–24, 2003, pp. 3477–3496.

[67] Martiny, M., Schulz, A., and Witting, S., "Full-Coverage Film Cooling Investigations: Adiabatic Wall Temperature and Flow Visualization," ASME Paper No. 95 Wa/HT-4, 1995.

[68] Andrews, G. E., Khalifa, I. M., Asere, A. A., and Bazdidi-Tehrani, F., "Full Coverage Effusion Film Cooling with Inclined Holes," American Society of Mechanical Engineers Paper No. 95-GT-247, 1995.

[69] Amer, A. A., Jobran, B. A., and Hamdan, M. A., "Comparison of Different Two-Equation Turbulence Models for Prediction of Film Cooling from Two Rows of Holes," *Numerical Heat Transfer, Part A, Applications*, Vol. 21, 1992, pp. 143–162.

[70] Jubran, B. A., "Correlation and Prediction of Film Cooling from Two Rows of Holes," *Journal of Turbomachinery*, Vol. 111, No. 2, 1989, pp. 502–509.

[71] Sasaki, M., Takahara, K., Kumagai, T., and Hanano, M., "Film Cooling Effectiveness for Injection from Multirow Holes," *Journal of Engineering for Power*, Vol. 101, No. 4, 1979, pp. 101–108.

[72] Mayle, R. E., and Camarata, F. J., "Multihole Cooling Film Effectiveness and Heat Transfer," *Journal of Heat Transfer*, Vol. 97, Jan. 1975, pp. 534–538.

[73] Walters, D. K., and Leylek, J. H., "Impact of Film-Cooling Jets on Turbine Aerodynamic Losses," *Journal of Turbomachinery*, Vol. 122, Nov. 2000, pp. 537–545.

[74] Hass, W., Rodi., W., and Schonung, B., "The Influence of Density Difference Between Hot and Coolant Gas on Film Cooling by a Row of Holes: Prediction and Experiments," *Journal of Turbomachinery*, Vol. 114, No. 3, 1992, pp. 747–755.

[75] Mehendale, A., and Han, J., "Influence of Main Stream Turbulence on Leading Edge Film Cooling Heat Transfer," *Journal of Turbomachinery*, Vol. 114, No. 10, 1992, pp. 705–715.
[76] Kohli, A., and Bogard, D., "Effects of Very High Free-Stream Turbulence on the Jet-Mainstream Interaction in a Film Cooling Flow," *Journal of Turbomachinery*, Vol. 120, No. 4, 1998, pp. 785–790.
[77] Cutbirth, J. M., and Bogard, D. G., "Evaluation of Pressure Side Film Cooling with Flow and Thermal Field Measurements, Part 2: High Mainstream Turbulence," *Journal of Turbomachinery*, Vol. 124, No. 4, 2002, pp. 678–685.
[78] Jenkins, S., Varadarajan, K., and Bogard, D., "The Effects of High Mainstream Turbulence and Turbine Vane Film Cooling on the Dispersion of a Simulated Hot Streak," *Journal of Turbomachinery*, Vol. 126, No. 1, 2004, pp. 203–212.
[79] Ou, S., Mehendale, A. B., and Han, J. C., "Influence of High Mainstream Turbulence on Leading Edge Film Cooling Heat Transfer: Effect of Film Hole Row Location," *ASME90-WA/HT-5, ASME Winter Annual Meeting*, ASME1990.
[80] John, P. O., and Haji-Sheikh, A., "Numerical Study of Film Cooling in Supersonic Flow," *AIAA Journal*, Vol. 30, No. 10, 1992, pp. 2426–2433.
[81] Kanda, T., Ono, F., Takahashi, M., Saito, T., and Wakamatsu, Y., "Experimental Studies of Supersonic Film Cooling with Shock Wave Interaction," *AIAA Journal*, Vol. 34, No. 2, 1996, pp. 265–271.
[82] Aupoix, B., Mignosi, A., and Viala, S., "Experimental and Numerical Study of Supersonic Film Cooling," *AIAA Journal*, Vol. 36, No. 6, 1998, pp. 915–923.
[83] Ligrani, P. M., Saumweber, C., Schulz, A., and Wittig, S., "Shock Wave-Film Cooling Interactions in Transonic Flows," *Journal of Turbomachinery*, Vol. 123, No. 6, 2001, pp. 788–797.
[84] Kost, F., and Nicklas, M., "Film-Cooled Turbine Endwall in a Transonic Flowfield, Part 1: Aerodynamic Measurements," *Journal of Turbomachinery*, Vol. 123, No. 4, 2001, pp. 709–719.
[85] Nicklas, M., "Film-Cooled Turbine Endwall in a Transonic Flowfield, Part 2: Heat Transfer and Film-Cooling Effectiveness," *Journal of Turbomachinery*, Vol. 123, No. 4, 2001, pp. 720–729.
[86] Javadi, A., Javadi, K., and Taeibi-Rahni, M., "Simulation of Film Cooling of Gas Turbine Blades," Aerospace Research Inst., TR ARI-82-31-FCG-4-2-1, Ministry of Science, Research and Technology, Tehran, Iran, 2002.
[87] Javadi, A., Javadi, Kh., Taeibi-Rahni, M., Darbandi, M., Aavani, Kh., and Mahjoob, S., "New Approach in Film Cooling on Gas Turbine Blades Using Combination of Suction/Blowing Flows," Aerospace Research Inst., TR ARI-82-31-FCG-4-1-1, Ministry of Science, Research and Technology, Tehran, Iran, 2003.
[88] Javadi, Kh., Taeibi-Rahni, M., Darbandi, M., "Jet into Cross Flow Boundary Layer Control: An Innovation in Gas Turbine Blade Cooling," *The 35th AIAA Fluid Dynamics Conference and Exhibition*, AIAA, Reston, VA, 2005.
[89] Javadi, A., Javadi, K., Taeibi-Rahni, M., and Darbandi, M., "A New Approach to Improve Film Cooling Effectiveness Using Combined Jets," Gas Turbine Society of Japan, TS-069, Tokyo, 2003.
[90] Javadi, Kh., Taeibi-Rahni, M., and Javadi, A., "New Method to Control Turbulent Jet-into-CrossFlow Interaction-Skin Friction Drag Reduction," *The 9th Fluid Dynamics Conference*, Shiraz Univ., Shiraz, Iran, 2004.
[91] Launder, B. E., and Shima, N., "Second-Moment Closure for the Near-Wall Sublayer: Development and Application," *AIAA Journal*, Vol. 27, No. 10, 1989, pp. 1319–1325.
[92] Daly, B. J., and Harlow, F. H., "Transport Equations of Turbulence," *Physics of Fluids*, Vol. 13, No. 11, 1970, pp. 2634–2649.
[93] Hanjalic, K., and Launder, B. E., "A Reynolds Stress Model of Turbulence and Its Application to Thin Shear Layers," *Journal of Fluid Mechanics*, Vol. 52, No. 4, 1972, pp. 609–638.
[94] Launder, B. E., Reece, G. J., and Rodi, W., "Progress in the Development of a Reynolds-Stress Turbulence Closure," *Journal of Fluid Mechanics*, Vol. 68, No. 3, 1975, pp. 537–566.
[95] Gibson, M. M., and Launder, B. E., "Ground Effects on Pressure Fluctuations in the Atmospheric Boundary Layer," *Journal of Fluid Mechanics*, Vol. 86, No. 3, 1978, pp. 491–511.
[96] Lumley, J. L., and Khajeh-Nouri, B. J., "Computational Modeling of Turbulent Transport," *Advances in Geophysics*, Vol. 18A, 1974, pp. 169–92.
[97] Fu, S., Launder, B. E., and Leschziner, M. A., "Modeling Strongly Swirling Recirculating Jet Flow with Reynolds Stress Transport Closures," *The Sixth Symposium on Turbulent Shear Flows*, 1987.
[98] Hwang, R. R., and Jaw, S. Y., "Second-Order Closure Turbulence Models: Their Achievements and Limitations," *Proceedings of the National Science Council, A: Physical Science and Engineering*, Vol. 22, No. 6, 1998, pp. 703–722.
[99] Menter, F. R., "Two-Equation Eddy-Viscosity Turbulence Models for Engineering Applications," *AIAA Journal*, Vol. 32, No. 8, 1994, pp. 1598–1605.
[100] Versteeg, H. K., and Malalarekara, W., *An Introduction to Computational Fluid Dynamics*, Addison Wesley Longman, Reading, MA, 1996, pp. 77–78.
[101] Davidson, L., *An Introduction to Turbulence Models*, Chalmers Univ. of Technology, Gothenburg, Sweden, 2003, Rept. No. 97/2.
[102] Thompson B., and Whitelaw, J., "Characteristics of a Trailing Edge Flow with Turbulent Boundary-Layer Separation," *Journal of Fluid Mechanics*, Vol. 157, Aug. 1985, pp. 305–326.
[103] Davidson, L., "Prediction of the Flow Around an Airfoil Using a Reynolds Stress Transport Model," *Journal of Fluids Engineering*, Vol. 117, 1995, pp. 50–57.
[104] Davidson, L., "Reynolds Stress Transport Modeling of Shock-Induced Separated Flow," *Computers and Fluids*, Vol. 24, No. 3, 1995, pp. 253–268.

R. So
Associate Editor